Molecular glues of the regulatory ChREBP/14-3-3 complex protect beta cells from glucolipotoxicity.

Authors

Liora S. Katz[1*], Emira J. Visser[2*], Kathrin F. Plitzko[3*], Marloes Pennings[2*], Peter J. Cossar[2], Isabelle L. Tse[1], Markus Kaiser[3], Luc Brunsveld[2#], Donald K. Scott[1#], Christian Ottmann[2#]

[*] Contributed equally; [#] Corresponding authors

Affiliations

[1] Diabetes, Obesity and Metabolism Institute and Mindich Child Health and Development Institute, Icahn School of Medicine at Mount Sinai, One Gustave L. Levy Place, Box 1152, New York, 10029, USA

[2] Laboratory of Chemical Biology, Department of Biomedical Engineering and Institute for Complex Molecular Systems, Eindhoven University of Technology, Den Dolech 2, 5612 AZ Eindhoven, The Netherlands

[3] Chemical Biology, Center of Medical Biotechnology, Faculty of Biology, University of Duisburg-Essen, Duisburg, Germany

Disclosures

US provisional patent application No. 63/523,289 – Pennings M.A.M., Katz L.S. Ottmann C, Scott D.K, Visser E.J. Plitzko K.F, Kaiser M Cossar P.J, Brunsveld, L. Small-molecule stabilizers of the ChREBP–14-3-3 interaction with cellular activity. United States Patent and Trademark Office, June 2023

The authors declare the following competing financial interest(s): L.B. and C.O. are founders of Ambagon Therapeutics. L.B. is a member of Ambagon's scientific advisory board, C.O. is employee of Ambagon.

Graphical Abstract

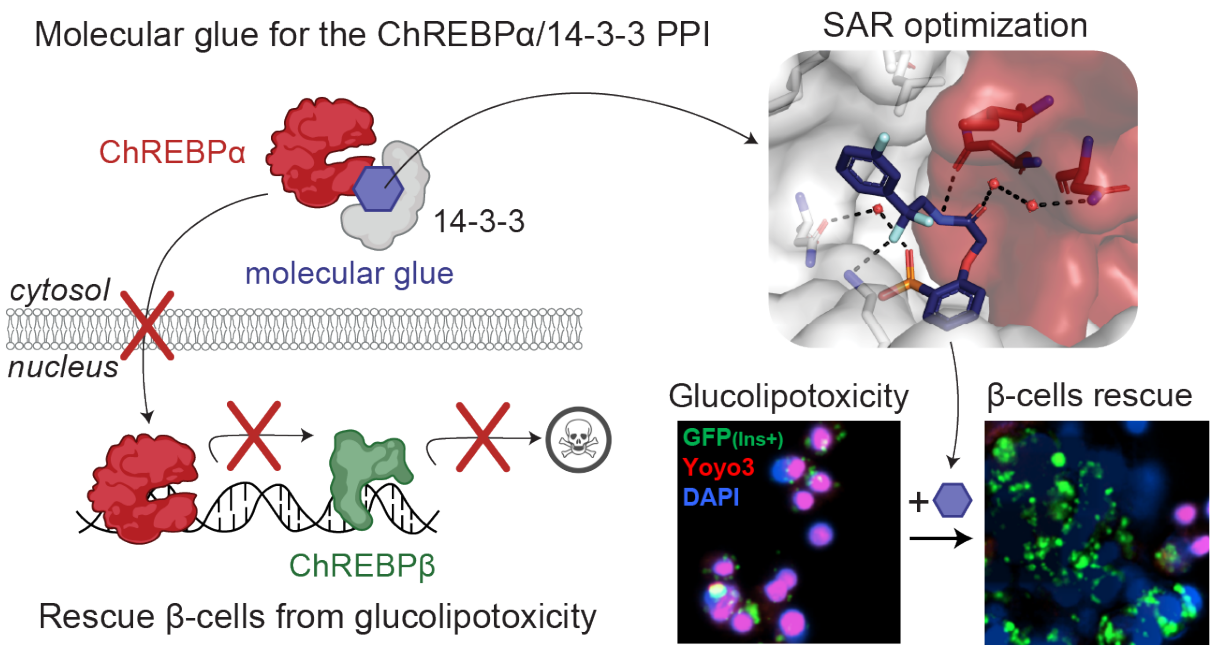

Abstract

The Carbohydrate Response Element Binding Protein (ChREBP) is a glucose-responsive transcription factor (TF) that is characterized by two major splice isoforms (α and β). In acute hyperglycemia, both ChREBP isoforms regulate adaptive β-expansion; however, during chronic hyperglycemia and glucolipotoxicity, ChREBPβ expression surges, leading to β-cell dedifferentiation and death. 14-3-3 binding to ChREBPα results in its cytoplasmic retention and concomitant suppression of transcriptional activity, suggesting that small molecule-mediated stabilization of this protein-protein interaction (PPI) via molecular glues may represent an attractive entry for the treatment of metabolic disease. Here, we show that structure-based optimizations of a molecular glue tool compound led not only to more potent ChREBPα/14-3-3 PPI stabilizers but also for the first time cellular active compounds. In primary human β-cells, the most active compound stabilized the ChREBPα/14-3-3 interaction and thus induced cytoplasmic retention of ChREBPα, resulting in highly efficient β-cell protection from glucolipotoxicity while maintaining β-cell identity. This study may thus not only provide the basis for the development of a unique class of compounds for the treatment of Type 2 Diabetes but also showcases an alternative 'molecular glue' approach for achieving small molecule control of notoriously difficult targetable TFs.

Introduction

Type 2 diabetes (T2D) poses an escalating burden on global health and economy. In 2021 537 million adults worldwide had diabetes, and this is expected to rise to 693 million by 2045 (1) or even 1.31 billion by 2050 (2-4), making it one of the leading causes of global morbidity (5). Both major types of diabetes are characterized by insufficient β-cell mass to meet the increased demand for insulin. T2D develops due to decreased insulin response (6), triggering a vicious cycle of increased insulin demand and decreased peripheral tissue response. While lifestyle adjustments can alleviate insulin resistance (7, 8), inadequate hyperglycemic control can lead to β-cell exhaustion, dedifferentiation, and eventual demise due to metabolic stress. This final stage is irreversible due to the restricted proliferative capacity of adult β-cells. Current T2D therapies mainly target insulin resistance and secretion, yet many T2D patients eventually become insulin dependent due to the loss of β-cells. Preventing the loss of β-cell mass remains one of the most important unmet needs in the armamentarium for the treatment of diabetes.

An emerging potential target to treat T2D is the glucose-responsive transcription factor (TF) Carbohydrate Response Element Binding Protein [ChREBP, (9-14)]. ChREBP is a key mediator in the response to glucose in pancreatic β-cells, controlling the expression of glycolytic and lipogenic genes (14). Small molecule modulation of ChREBP function may thus represent a promising approach to combat T2D; however, many TFs such as ChREBP are known as notoriously difficult to target with small molecules due to their lack of suitable ligand binding sites (15). However, several proteins interact with ChREBP to regulate its activation mechanism (16), including the 14-3-3 protein (17, 18). The protein-protein interaction (PPI) between ChREBP and 14-3-3 potentially offer long-sought entries to address ChREBP via molecular glues (19-22). The “hub” protein 14-3-3 is involved in numerous signaling pathways, as well as in the pathophysiologic state of diabetes (23-25). Molecular scaffold proteins belonging to the 14-3-3 protein family are widely conserved among eukaryotes (26-28). In mammals, this family comprises seven isoforms, namely, β, γ, ζ, η, τ, σ, and ε (29). In the context of pancreatic β-cells, 14-3-3 proteins are integral to the regulation of insulin secretion,

cell proliferation, and survival (25). They contribute to maintaining glucose homeostasis and influence key aspects of the cell cycle, impacting β-cell mass (24, 30). The diverse functions of 14-3-3 proteins encompass their involvement in mitochondrial activity (24, 31), cell cycle progression (25, 32), contribution to apoptosis and cell survival pathways (23). ChREBP interacts with 14-3-3 via an alpha helix in its N-terminal domain (residues 117-137), which is one of the few known phosphorylation-independent 14-3-3 binding motifs (33-35). The molecular basis of this PPI has been studied by X-ray crystallography, revealing the presence of a free sulfate or phosphate ion binding in the 14-3-3 phospho-accepting pocket that interacts with both proteins (**Fig. S1a**) (36). Adenosine monophosphate (AMP) has also been reported to bind to this phospho-accepting pocket, weakly stabilizing the protein complex and enhancing the 14-3-3-mediated cytoplasmic sequestration of ChREBP (**Fig. S1b**) (37). Next to inorganic phosphate and AMP, ketone bodies regulate ChREBP activity by increasing its binding to 14-3-3 (17, 37-39). This may suggest that small-molecule stabilizers – molecular glues – of the ChREBP/14-3-3 PPI are potentially valuable tools to suppress glucolipotoxicity in T2D by inhibiting the transcriptional activity of ChREBP, thereby overcoming the current limitations of 'direct' targeting of TF functions.

MLXIPL, the gene that expresses ChREBP, produces two major splice isoforms: ChREBPα and ChREBPβ. The ChREBPα isoform is the full length-isoform, containing the low glucose inhibitor domain (LID, including the nuclear export signal (NES)) at its N-terminal region. One of the mechanisms that retains ChREBPα in the cytosol is *via* its interaction with 14-3-3 (**Fig. 1a**) (17, 37-39). ChREBPβ lacks this N-terminal domain, resulting in a nuclear, constitutively active, hyper-potent TF (40-43). In healthy conditions, glucose flux leads to dissociation of CHREBPα from 14-3-3 resulting in its translocation to the nucleus and induction of ChREBPβ transcription, ultimately leading to glucose-stimulated β-cell proliferation to meet the demand for insulin (**Fig. 1b**). However, under prolonged hyperglycemic conditions, a robust positive feedback loop is triggered in which the newly produced ChREBPβ binds to its own promoter sites leading to even more ChREBPβ synthesis eventually resulting in glucolipotoxicity and β-

cell apoptosis (**Fig. 1c**) (17, 37-39). These molecular mechanisms suggest that small molecule stabilization of the ChREBPα/14-3-3 PPI via a suitable molecular glue may however prevent the nuclear import of ChREBPα under prolonged hyperglycemic conditions and thereby avert glucolipotoxicity (**Fig. 1d**). Indeed, our groups recently developed biochemically active stabilizers of the ChREBPα/14-3-3 PPI (22); these compounds were however only moderately active and more importantly lacked cellular activity, preventing cellular validation and downstream analyses of our hypothesis (22). Here, we aimed to further improve these ChREBPα/14-3-3 PPI small-molecule stabilizers by using structure-activity relationship (SAR) analysis. This resulted in small-molecule stabilizers with a cooperativity factor (α) up to 220 for the ChREBPα/14-3-3 PPI. The introduction of a *geminal*-difluoro group into the pharmacophore not only significantly enhanced their stabilization efficiency, most probably by slight bending of the pharmacophore arrangement, but was also crucial for obtaining cellular activity. X-ray crystallography confirmed engagement of the molecular glues at the composite interface formed by the 14-3-3 binding peptide motif of ChREBPα and 14-3-3. Immunofluorescence showed retention of ChREBPα, by 14-3-3, in the cytoplasm of primary human β-cells upon addition of the stabilizers. Concomitantly, the transcriptional activity of ChREBPα was suppressed, hence preventing the upregulation of ChREBPβ in response to glucose and glucolipotoxicity. By exploiting this mechanism of action, β-cells were rescued from glucolipotoxicity, both in terms of viability and in terms of β-cell identity, including insulin production, by keeping ChREBP transcriptionally inactive at high glucose levels. This study provides the foundation for a potential new class of compounds for regulating ChREBP activity in T2D (22, 37, 44-48).

Results

Focused library based on 1 established a crucial SAR

To investigate the hypothesis that cytosolic sequestration of ChREBPα via molecular glue stabilization of the ChREBPα/14-3-3 PPI inhibits downstream glucotoxicity and β-cell apoptosis it was critical that our previously discovered stabilizer **1** (**Fig. 2a**) was first optimized to improve activity, but more importantly cellular efficacy. Stabilizer **1** was previously found to bind to the ChREBPα-peptide/14-3-3β interface (**Fig. S2a-c**) (22). A challenge to optimization of **1** was the poor resolution of the ligand's electron density in the X-ray co-crystal structure, particularly around the phenyl ring and linker of **1**. This poor electron density limited structure-guided optimization and indicated sub-optimal PPI stabilization (**Fig. S2d**). To address this technical challenge our efforts were direct towards the development of an alternative crystallization approach. Gratifyingly, this novel co-soak crystallization approach (see ESI) resulted in a new co-crystal structure with an improved resolution of 1.6 Å. The improved resolution enabled a more reliable model building, including the atomic fitting of the phenyl ring and ethylamine linker of **1**. (**Fig. 2a, S2e**). In addition to the phosphonate of **1** interacting with the phosphate-accepting pocket of 14-3-3 (R56, R129, Y130), and R128 of ChREBPα (**Fig. 2b**), it was now observed that both the phenyl and phenyl phosphonate rings of **1** make hydrophobic contacts with side chains of both 14-3-3 and ChREBPα. Further, an intramolecular hydrogen bond between the amide moiety and the phosphonate group of **1** was resolved. Finally, the improved resolution of this novel crystal structure enabled detection of a water-mediated hydrogen bond between the carbonyl amide of **1** and the main chain amide of I120 of ChREBPα (**Fig. 2b**). Subsequent Fluorescence Anisotropy (FA) measurements revealed that compound **1** stabilized the ChREBPα/14-3-3 complex with cooperativity factor (α) of 35 (**Fig. 2c**).

With structural characterization of the ternary ChREBPα/14-3-3/**1** complex in hand, attention was shifted to the optimization of compound activity. To gain a greater SAR understanding, a

focused library was synthesized aiming to improve the stabilization efficiency and selectivity for this class of molecular glues, in which compounds were compared based on their EC_{50} value derived from FA based compound titrations (**Fig. 2d, S3d, S4, S5, Table S1**) (49-51). To mimic the structure of the natural stabilizer **AMP**, the phenyl substituent of **1** was replaced by a purine (**2**, **3**, **4**). However, these modifications were not tolerated. Similarly, no stabilization was observed upon replacement of the phenyl moiety with either an indole (**5**), or a cyclohexane moiety (**6**), while naphthalene groups (**7**, **8**) led to slightly more active compounds. Extension of the phenyl group with a methylpyridine functional group (**9, 10, 11**) increased the stabilization efficiency, with the N-2 position (**9**, EC_{50} = 7.6 ± 0.5 μM) eliciting the greatest response. Substitutions at the central acetamide were not tolerated (**12, 13, 14**). Furthermore, systematic shifting of the phosphonate group along the phenyl phosphonate ring showed that the *ortho* position is most favorable (**1, 15, 16**). Interestingly, replacement of the phosphonate with a phosphate group was tolerated (**17**, **18**, **19**) and the *para* positioned analog led to improved compound activity (EC_{50} = 17.4 ± 3.2 μM). Conversion of the phenyl phosphonate into a benzyl phosphonate was however not tolerated (**20**, **21**, **22**). Phosphonate mimics, e.g. a boronic acid (**23**) or a sulfonamide (**24**) group were also inactive compounds. Lastly, we focused on modifications of the alkyl fragment of the phenyl ethyl amine moiety. Investigation of the SAR around the ethylene linker showed that replacement of the ethylene linker with a constrained (1*R*, 2*S*) cyclopropyl ring (**25**, EC_{50} = 17.6 ± 1.7 μM) elicited similar activity to **1**, while stereoisomers **26** (1*S*, 2*R*) and **27** (1*R*, 2*R*) were not tolerated. Furthermore, ring expansion to the cyclopentyl ring (**28**, 1*R*, 2*R*) was inactive and installation of a cyclobutyl (**29**) or *geminal*-dimethyl groups (**31**) resulted in diminished activity relative to **1**. Interestingly, the introduction of a *geminal*-difluoro group however significantly enhanced (six-fold relative to **1**) the stabilization of the ChREBPα/14-3-3 PPI, resulting in the best stabilization observed so far (**30**, EC_{50} = 5.8 ± 0.4 μM). Unfortunately, this analog was not amendable for phosphonate replacement with a sulfonamide or boronic acid, since this resulted in inactivity (**58**, **68**, **Table S2**). Merging the two best stabilizers (**9** and **30**) resulted in analog **73** with a similar EC_{50} value compared to each individual substitution (**73**, EC_{50} = 11.0 ± 1.5 μM, **Table**

S3). Co-crystallization of ChREBPα and 14-3-3 was successful for **30**, showing a clear density of both the ChREBPα peptide and **30** (**Fig. S6a**). Overlaying the crystal structure of **30** with **1** revealed a high conformational similarity of 14-3-3σ and the ChREBPα peptide, with a comparable positioning of the phosphonate of **30** in the ChREBPα/14-3-3 phospho-accepting pocket (**Fig. 2e, 2f**). The *geminal*-difluoro group of **30** was, however, directed downwards into the 14-3-3 binding groove, causing an alternative bend of the phenyl ethyl amine moiety (**Fig. 2f**). Both fluorine atoms form interactions with 14-3-3σ; one directly contacts K49 and the other engages in a water-mediated polar interaction with N175 (**Fig. 2g**), thereby recapitulating other literature reports showing that fluorinated small molecules can form potent hydrogen bonds (49-51). Additionally, due to the alternative bend of the linker, the amide of **30** was now positioned to interact with N123 and N124 of ChREBPα (**Fig. 2g**). These additional contacts of the molecular glue with both 14-3-3 and ChREBPα explain the increase in ternary complex formation by the introduction of the *geminal*-difluoro group.

Fluorination of compounds improves stabilization potency

Encouraged by the enhanced stabilizing activity of the fluorinated analog **30**, a focused library of fluorinated compounds was next synthesized and compared to their non-fluorinated analogs (**Fig. 3a, Table S3**). Fluorination of analogs increased their stabilization potency consistently across all library members. Even the previously inactive *p*-Cl (**32**) and *p*-Br (**33**) substituted compounds now elicited a high activity when combined with the *geminal*-difluoro group substitution (**40:** EC_{50} = 6.6 ± 0.9 μM, **41**: EC_{50} = 4.1 ± 0.4 μM, respectively). The fluorine functionality has a common place in medicinal chemistry as reflected by 20-25% of drugs in the pharmaceutical pipeline containing at least one fluorine atom (52, 53). Introduction of a fluoro group at the *meta* position of the phenyl ring even further improved compound activity (**43**: EC_{50} = 3.8 ± 0.2 μM). Additional to single fluoro-substitutions at the phenyl ring of **30**, double fluoro-substituted analogs were synthesized (panel IV in **Fig. 3a**). A 2,4-difluoro substitution resulted in the most potent stabilizer observed so far (**53**, EC_{50} = 3.1 ± 0.6 μM).

Two-dimensional FA titrations were performed to investigate the cooperativity in ChREBPα/14-3-3/stabilizer complex formation. 14-3-3β was titrated to FITC-labeled ChREBPα peptide (10 nM) in the presence of different, but constant, concentrations of **30**, **43** or **53** (0–500 μM), showing up to 138-fold, 60-fold and 111-fold increase in stabilization, respectively, by the three molecular glues (**Fig. 3b, 3c, S7a**). The change in apparent K_D of the ChREBPα/14-3-3 complex, over different concentrations of stabilizer (**Fig. S7b**), showed that all three fluorinated compounds (**30**, **43** and **53**) elicit a similar stabilizing profile, with a 2.4- to 6-fold increase in stabilization compared to the non-fluorinated parent analog **1**. The combined two-dimensional data was fitted using a thermodynamic equilibrium model (**Fig. S8**) (54) to determine the cooperativity factors (α), and the intrinsic compound affinities to 14-3-3 (K_D^{II}). All three fluorinated compounds showed increased cooperativity (α = 220 (**30**), 72 (**43**), 126 (**53**)) compared to their defluorinated parent compound **1** (α = 35), while their intrinsic affinity for 14-3-3 was barely affected (K_D^{II} = 168 μM, 162 μM, 110 μM for **30**, **43**, **53** and 161 μM for **1**). This indicates that the compound optimization has mainly improved the interaction with ChREBPα and not the binding affinity to 14-3-3. Of note, the mean squared error landscape of the two fitted parameters showed for some stabilizers that the α and K_D^{II} parameters are interconnected, meaning that a weaker intrinsic affinity, K_D^{II}, correlates to an increased cooperativity factor, α. (**Fig. S8**).

Phosphate- and phosphonate-based compounds may also act as inhibitors of other 14-3-3-client protein complexes, often acting as low micromolar (IC_{50} ~ 1-20 μM) inhibitors (54-56). To test the specificity of the ChREBPα/14-3-3 PPI stabilizers, we selected an array of eight representative 14-3-3 client-derived peptide motifs with differentiating binding sequences and included internal binding motifs BRAF (57), CRAF (58), p65 (59), USP8 (60, 61), one C-terminal binding motif ERα (62), one special binding mode Pin1 (63) and another reported non-phosphorylated motif ExoS (34). Strikingly, all three compounds (**30**, **43**, **53**) displayed a high selectivity for stabilizing ChREBPα, without affecting any other client peptide up to 100 μM (**Fig. 3d, S7c**). These data demonstrate the highly selective nature of the molecular glue

activity of these compounds by addressing a unique pocket only present in the ChREBPα/14-3-3 complex and via a stabilization mechanism, involving a large cooperativity effect.

Crystallization of the new fluorinated compounds with the ChREBPα/14-3-3σ complex was also successful for **42** and **43**, resulting in a clear density for the entire molecule (**Fig. S6b, c**). A crystallographic overlay with **30** revealed an additional conformational 'clamping' effect of helix-9 of 14-3-3σ in the presence of **43** (**Fig. 3e**), causing the hydrophobic residues of 14-3-3 (I219, L218) to be closer to the phenyl ring of **43**. This clamping effect of helix-9 is in line with previous observations for molecular glues with high cooperativity factors, for other 14-3-3 PPIs (64). A more detailed analysis showed that the *meta*-fluoro group of **43** is positioned at the rim of the hydrophobic interface of 14-3-3 and ChREBPα (**Fig. 3f**). The rest of stabilizer **43** has similar interactions with both ChREBPα and 14-3-3 as **30** (**Fig. 3g, S9**). An *ortho*-fluoro substitution at the phenyl ring was less favorable (**42**, EC_{50} = 9.6 ± 1.1 μM) although it did result in a similar 'clamping' effect of helix-9 of 14-3-3 (**Fig. S10**). This *ortho* substituted fluoro was not positioned at the rim of the ChREBPα/14-3-3 interaction interface, instead it made a polar interaction with N175 of 14-3-3 (**Fig. S10**). While no crystal structure could be solved for the double fluoro-substituted analog **53**, the structure of **43** shows room for a fluoro-substitution at the *para* position of its phenyl ring, explaining the high potency of **53** (**Fig. 3g**). Likely, the electron withdrawing effects of the fluorine substitutions are enhancing hydrophobic contacts with the hydrophobic amino acids at the roof of the 14-3-3 groove. Concluding, fluorination of the scaffold enhanced stabilizing efficiency of the ChREBPα/14-3-3 complex, by strengthening the interactions at the rim of the PPI interface.

Molecular glues stabilizing the ChREBPα/14-3-3 interaction rescue human β-cells from glucolipotoxic death

We tested six compounds (**1**, **12**, **30**, **43**, **53**, **66**) for cytotoxicity and their ability to protect β-cells from glucolipotoxicity (summarized in **Fig. 4a**). Compound **1**, our previously reported

parent compound that was moderately active in the biochemical assay, displayed cytotoxicity in INS-1 cells. In contrast, compounds **30**, **43** and **53** which were all active in biochemical assays, demonstrated no unspecific cytotoxicity in INS-1 cells and also protected the β-cells from glucolipotoxicity, turning them into candidates for further cellular evaluation. Compounds **12** and **66**, which served as control compounds, were not active in the biochemical assay and were also neither generally cytotoxic nor rescued the cells from glucolipotoxicity. To test the efficacy of our compounds in mitigating β-cell death from glucolipotoxicity, we conducted dose-response experiments in rat insulinoma, β-cell-like INS-1 cells. We observed a significant attenuation of cell death in response to glucolipotoxic conditions at 5 and 10 μM of active compounds **30**, **43**, and **53**, but not in the presence of the inactive compounds **12** or, **66** (**Fig. S11**). To investigate cadaveric human islets, we optimized the single-cell and population-level analyses using real-time kinetic labeling (SPARKL) assay (65, 66), that measures the kinetics of overall proliferation (cell count, using NucBlue) or cell death rates (using YoYo3) specifically in β-cells using the rat insulin promoter (RIP)-ZSGreen adenovirus ((67) (**Fig 4b, Fig S11**)). The active compounds (**30**, **43**, **53**) all exhibited a remarkable decrease in β-cell death in glucolipotoxic conditions, as observed in **Fig 4c, 4d, 4e** while the 'inactive' control compounds also in this assay showed no activity. Notably, for all five tested compounds, there was no discernible impact on β-cell number, indicating that over the course of 72 h, no meaningful proliferation occurred in treatment groups (**Fig 4f, 4g**). Our method was validated using TUNEL staining at 48 h using 10 μM **43** to show similar cell death patterns as the kinetic measurement (**Fig S12**). Indeed, **43**, which we focus on for the rest of this study, also prevented glucose-stimulated proliferation, confirming our previous studies (14, 42, 43) and glucolipotoxic cell death in INS-1 cells (**Fig S13**). Together, these studies demonstrated that the three active compounds (**30**, **43**, **53**) prevent β-cell death in the context of glucolipotoxicity.

Compound 43 stabilizes the ChREBPα/14-3-3 interaction *in situ* preventing ChREBPα's nuclear translocation in response to glucose or glucose + palmitate

To explore the mechanism by which **43** acts *in cellulo* as a molecular glue, we performed three sets of experiments. First, a proximity ligation assay (PLA) was employed in INS-1 cells using an antibody against ChREBPα and a pan 14-3-3 antibody. PLA assays show a fluorescent signal only when proteins are in close (<40 nm) and stable proximity to each other (68). In low glucose, we observed a strong interaction between 14-3-3 and ChREBPα. By contrast, following exposure to high glucose for 30 min, ChREBPα no longer interacted with 14-3-3, but the interaction was restored after 2 h (**Fig 5a**). These observations are consistent with our previous study showing that ChREBPα transiently enters the nucleus to begin the feed-forward induction of ChREBPβ (42). Remarkably, in the presence of **43**, the interaction between 14-3-3 and ChREBPα remained unchanged at high glucose concentrations, thus confirming that **43** stabilized the interaction between 14-3-3 and ChREBPα in high glucose. In a second set of experiments, in which nuclear localization of ChREBPα was studied using a ChREBPα-specific antibody, we again found the same dynamics; ChREBPα entered the nucleus after 30 min of high glucose and exited the nucleus after 2 h. However, **43** blocked the transient translocation of ChREBPα in response to glucose (**Fig. 5b, 5c**). Under glucolipotoxic conditions (20 mM glucose + 500 μM palmitate), we observed a similar translocation of ChREBPα to the nucleus after 30 min, however, the nuclear clearance of ChREBPα under glucolipotoxic conditions took longer compared to high glucose alone (**Fig. 5d, 5e**). After 48 h under glucolipotoxic conditions, ChREBPα was no longer in the nucleus (**Fig. 5f.g**). Once again, by stabilizing its interaction with ChREBPα, compound **43** prevented nuclear translocation of ChREBPα under the more stimulating glucolipotoxicity conditions (**Fig 5d, 5e**). Because our nuclear translocation studies are based on immunodetection, this positive outcome could be a result of epitope masking, e.g. by a ChREBPα interaction with the transcription machinery or other heteropartners, which could block antibody binding.

Therefore, a third approach used CRISPR/Cas9 engineered INS-1 cells (42) wherein fluorescent tags to the 5′ and 3′ ends of ChREBP were added. An mCherry tags the N-terminal LID domain, which identifies ChREBPα exclusively, and an eGFP tag on the C-terminus represents both ChREBPα and ChREBPβ. In these cells, ChREBPα appears as yellow (red+green), and ChREBPβ appears green. Compound **43** clearly prevents the built up of ChREBPβ in both high glucose and glucolipotoxic conditions, thus confirming the immunostaining results (**Fig. 5f, 5g**). Together, these studies demonstrate that **43** stabilizes the interaction of 14-3-3 and ChREBPα under conditions of hyperglycemia and glucolipotoxicity.

Effect of stabilizers on ChREBP downstream genes and preservation of β-cell identity

Next, we assessed the effect of stabilizers on transcription of the ChREBP splice isoforms in human islets. While ChREBPα mRNA levels remained relatively stable in all conditions tested (**Fig. 6a**), ChREBPβ, which contains a well characterized ChoRE on its promoter (40, 43), was upregulated in response to high glucose, or to high glucose and high palmitate (glucolipotoxicity). Interestingly, compound **43** prevented upregulation of ChREBPβ both at mRNA level (**Fig. 6b**) and at protein level (**Fig. 6c, 6d**), indicating that inhibition of the nuclear translocation of ChREBPα by strengthening the ChREBPα/14-3-3 interaction with **43** is required for the blocking of the upregulation of glucose responsive genes such as ChREBPβ. TXNIP is another glucose responsive gene, which also contains a well characterized ChoRE (69-71) and its upregulation is implicated in oxidative stress and β-cell death (72-74). Promoter luciferase assays demonstrated that **43** prevents the glucose response of the TXNIP gene (**Fig. 6e**). Importantly, β-cell identity marker genes INS (**Fig. 6f**) and PDX1 (**Fig. 6g**) were both downregulated at the mRNA level in human islets exposed to glucolipotoxicity, consistent with the previously reported de-differentiation phenotype pertinent to β-cell demise (75-78). Yet, in the presence of **43** this de-differentiation was prevented (**Fig. 6f, 6g)**. Similarly,

immunostaining for PDX1 showed a marked decrease in PDX1 protein levels in glucolipotoxicity, which was rescued by **43** (**Fig. 6c, 6h**).

Discussion

The global epidemic of T2D necessitates the development of novel therapeutic and preventive strategies to arrest the progressive nature of this disease (79). ChREBP is an important regulator of glucose levels and is increasingly recognized as a potential target for T2D treatment (80). A small molecule regulation of its function is however challenging as TFs are notoriously difficult to target with 'classical' small molecules. Here, we sought to develop a molecular glue approach, based on the use of novel small molecule PPI stabilizers, molecular glues, for the ChREBPα/14-3-3 PPI. These compounds were then used to test if retention of ChREBPα in the cytoplasm may lead to a persistent, chemotherapeutically exploitable inactivation of its transcriptional activity. Via the development of cellularly active molecular glues, we were able to proof that this unconventional strategy for targeting TF functions via TF retention in the cytoplasm indeed resulted in the desired, consistent, and efficacious glucolipotoxicity rescue phenotype. We also did not observe significant cytotoxicity on a cellular level. Besides its implications for T2D therapy, we therefore believe that 14-3-3 or other scaffold-mediated retention of TFs in the cytoplasm via customized molecular glues may represent a broader chemotherapeutic approach that may also be extended to other, difficult to target TFs with medicinal relevance. This strategy also complements other non-conventional 'molecular glue' or PROTAC TF approaches such as TRAFTACs or other TF targeted degradation systems (81-83).

Our cellular active molecular glues simultaneously engage both protein partners in the composite ChREBPα/14-3-3 binding pocket, causing a cooperativity factor up to 100 for this PPI. The addition of *geminal*-difluoro groups increased the PPI stabilization efficiency significantly, overall leading to compounds with micromolar cellular potency. On a molecular

level, this enhanced PPI stabilization by fluorination of the molecular glues was achieved by stimulating the clamping of helix-9 of 14-3-3 and contacting hydrophobic amino acids at the interaction surface of the ChREBPα/14-3-3 complex. This molecular mechanism also resulted in a very high selectivity of the compounds for the stabilization of the ChREBPα/14-3-3 PPI over other 14-3-3-based PPIs. Selective interfacing of these molecular glues with amino acid residues that only occur in the context of this specific PPI complex, thus result both in a large cooperative effect for PPI stabilization and high selectivity. Combined, this high cooperativity and selectivity for the ChREBPα/14-3-3 PPI conferred cellular activity to our lead compound.

Our studies also shed further light on the function and suitability of ChREBP as a target in metabolic disease. As T2D progresses, there is a progressive decline in β-cell mass due to the metabolic overload associated with a diabetic environment. ChREBP has long been identified as a potential mediator of this decline, in part by activating the pro-oxidative protuberant, TXNIP (70, 84-86). Indeed, clinical trials have been launched with compounds that inhibit the induction of TXNIP in T1D (87-89). We recently described the destructive feed-forward production of ChREBPβ in β-cells in the context of prolonged hyperglycemia and diabetes (42, 87-89). Importantly, we found that deletion of the ChREBPβ isoform, using the Lox/Cre system, completely rescued β-cells from glucolipotoxicity. Here, we found molecular glues, which prevented ChREBPα from dissociating from 14-3-3 and initiating the feed-forward production of ChREBPβ, that were also remarkably effective at preventing cell death from glucolipotoxicity. One consequence of the retention of ChREBPα was that the molecular glues attenuated cell proliferation (**Fig. S13f**). This result was consistent with our previous findings that a modest induction of ChREBPβ is required for adaptive β-cell expansion (14, 42, 43). Considering molecular glues as a potential therapeutic, it is likely that preservation of β-cell mass is more clinically relevant compared to the loss of an extremely low proliferation rate of human β-cells (90, 91).

Nuclear shuttling of ChREBPα in response to glucose is not only regulated by 14-3-3, but also by numerous post translational modifications (11, 37, 41, 92, 93), as well as by interaction with importin α (94). Since 14-3-3 and importin α compete for the same ChREBP binding region, ChREBP/importin α-PPI inhibitors, as developed by Uyeda *et al*. (95), could potentially work synergistically with ChREBPα/14-3-3 stabilizers in suppressing the progression of T2D. Importantly, upregulation of ChREBPβ and downstream genes (i.e. TXNIP and/or DNL genes) are implicated not only in β-cell demise but also in kidney failure (96), cardiac hypertrophy (97), ischemic and cardiovascular diseases (98, 99), liver steatosis where ChREBP is involved in the pathophysiology (100), and NAFLD (101) in particular in high glucose setting. Inhibiting ChREBPβ and downstream genes might prove to be valuable not only for preserving β-cell mass but may also be therapeutic in other tissues for the previously listed conditions.

To summarize, we demonstrated the development of highly potent, selective, active stabilizers of the ChREBPα/14-3-3 PPI with a phosphonate chemotype active in both INS-1 cell lines and primary human islets. This new compound class possibly presents the first foundations for the development of novel therapeutics against T2D. More broadly, this work delineates a novel conceptual entry to the forthcoming discoveries of molecular glues, and we envision that 14-3-3 PPI stabilization can not only be applied for the interaction with ChREBP but can be translated to other TFs as well and offers an orthogonal strategy for hard-to-drug proteins and pathways in general.

Online content

Any methods, additional references, Nature Portfolio reporting summaries, source data, extended data, supplementary information, acknowledgements, peer review information; details of author contributions and competing interests; and statements of data and code availability are available upon request

Methods

Protein expression and purification. The 14-3-3βFL and ΔC, and 14-3-3σΔC isoform (full length and truncated C-terminus after T231 (ΔC to enhance crystallization)) containing a N-terminal His6 tag were expressed and purified as described previously (102-108).

Peptide Sequences. The N-terminal FITC labeled ChREBP-derived peptide (residues 117 – 142; sequence: RDKIRLNNAIWRAWYIQYVKRRKSPV-$CONH_2$) was synthesized via Fmoc solid phase peptide synthesis as described previously (102-108). N-terminal acetylated ChREBP peptide used for crystallization was purchased from GenScript Biotech Corp. Peptides used for selectivity studies were purchased from GenScript Biotech Corp with the following sequences: BRAF: (5-FAM-RDRSS(pS)APNVH-$CONH_2$) , CRAF: (5-FAM-QRST(pS)TPNVH-$CONH_2$) , ERα: (5-FAM-AEGPFA(pT)V-COOH), EXO-S: (5-FAM-KKLMFK(pT)EGPDSD-$CONH_2$), P65: (5-FAM-EGRSAG(pS)IPGRRS-$CONH_2$), PIN1: (5-FAM-LVKHSQSRRPS(pS)WRQEK-$CONH_2$), USP8: (5-FAM-KLKRSY(pS)SPDITQ-$CONH_2$).

Fluorescence Anisotropy measurements. Fluorescein labeled peptides, 14-3-3βFL protein, the compounds (100 mM stock solution in DMSO) were diluted in buffer (10 mM HEPES, pH 7.5, 150 mM NaCl, 0.1% Tween20, 1 mg/mL Bovine Serum Albumin (BSA; Sigma-Aldrich). Final DMSO in the assay was always 1%. Dilution series of 14-3-3 proteins or compounds were made in black, round-bottom 384-microwell plates (Corning) in a final sample volume of 10 µL in duplicates.

Compound Titrations were made by titrating the compound in a 3-fold dilution series (starting at 500 µM) to a mix of FITC labeled peptide (10 nM) and 14-3-3β (concentration at EC_{20} value of protein-peptide complex; 150 nM for ChREBP). For the selectivity studies concentration of 14-3-3β were: 300 nM for ERα, 3.65 µM for Exo-S, 10 µM for Pin1, 250 nM for USP8, 230 nM for B-RAF, 30 µM for P65 and 450 nM for C-RAF. Fluorescence anisotropy measurements were performed directly.

Protein 2D titrations were made by titrating 14-3-3β in a 2-fold dilution series (starting at 300 μM) to a mix of FITC-labeled peptide (10 nM) against varying fixed concentrations of compound (2-fold dilution from 500 μM), or DMSO. Fluorescence anisotropy measurements were performed directly.

Fluorescence anisotropy values were measured using a Tecan Infinite F500 plate reader (filter set lex: 485 ± nm, lem: 535 ± 25 nm; mirror: Dichroic 510; flashes:20; integration time: 50 ms; settle time: 0 ms; gain: 55; and Z-position: calculated from well). Wells containing only FITC-labeled peptide were used to set as G-factor at 35 mP. Data reported are at endpoint. EC_{50} and K_D values were obtained from fitting the data with a four-parameter logistic model (4PL) in GraphPad Prism 7 for Windows. Data was obtained and averaged based on two independent experiments.

Cooperativity Analysis. The cooperativity parameters for compound **1**, **30**, **43** and **53** for 14-3-3 and ChREBP were determined by using the thermodynamic equilibrium system as described previously (102-108). The data from 2D-titrations was provided to the model including the K_D^I = 1.5 μM, P_tot = 10 nM, and the variable concentrations of 14-3-3 and stabilizer at each data point. Fit parameters were given the following initial guess values: K_D^{II}: 500 μM, α: 100.

X-Ray crystallography data collection and refinement. A mixture of Ac-ChREBP peptide and compound (2 μL of 5 mM stock ChREBP peptide + 0.5 μL of 100 mM stock compound) was mixed in crystallization buffer (CB: 20 mM HEPES pH 7.5, 2 mM $MgCl_2$, 2 mM βME) to a final concentration of 4 μL. This was added to preformed 14-3-3σ/Peptide-C crystals at 4 °C that were produced as described previously (102-108). Single crystals were fished after 7 days of incubation at 4 °C, and flash-cooled in liquid nitrogen. Diffraction data was collected at either the Deutsche Elektronen-Synchrotron (DESY Petra III beamline P11 proposal 11011126 and 11010888, Hamburg, Germany (crystal structures of compound **1** and **30**), or at the European Synchrotron Radiation Facility (ESRF Grenoble, France, beamline ID23-2 proposal MX2268) (crystal structures of compound **43** and **42**). Initial data processing was performed at DESY

using XDS (109) or at ESRF using DIALS (110) after which pre-processed data was taken towards further scaling steps, molecular replacement, and refinement.

Data was processed using the CCP4i2 suite (111) (version 8.0.003). After indexing and integrating the data, scaling was done using AIMLESS (112). The data was phased with MolRep (113) using 4JC3 as a template. Presence of soaked ligands and ChREBP-peptide was verified by visual inspection of the Fo-Fc and 2Fo-Fc electron density maps in COOT (114) (version 0.9.6). If electron density corresponding to ligand and peptide was present, the ChREBP peptide was built in and the structure and restrains of the ligands were generated using AceDRG (115), followed by model rebuilding and refinement using REFMAC5 (116). The PDB REDO (117) server (pdb-redo.edu) was used to complete the model building and refinement. The images were created using the PyMOL Molecular Graphics System (Schrödinger LLC, version 2.2.3). For refinement statistics see **Table S4**.

The structures were deposited in the protein data bank (PDB) with IDs: **8BTQ** (compound **1**), **8C1Y** (compound **30**), **8BWH** (compound **42**) and **8BWE** (compound **43**).

Synthesis of SAR library for 1. Detailed synthetic procedures and characterization of compounds marked with a star (*) in Table S1 were described previously (22). The synthetic procedure and characterization of all remaining compounds are provided in the Supplemental Methods. Generally, all compounds obtained had been purified by reversed-phase high performance liquid chromatography (HPLC) and characterized by liquid chromatography mass spectrometry (LC-MS) and nuclear magnetic resonance (NMR; 400 MHz for ^{1}H NMR and 100 MHz for ^{13}C NMR). Compounds were prepared as 100 mM stock solutions in DMSO before use in experiments, and stored at -20 °C.

Cell lines. INS-1–derived 832/13 rat insulinoma cells were maintained in RPMI 1640 medium with 10% FBS, 10 mM HEPES, 2 mM L-glutamine, 1 mM sodium pyruvate, and 50 mM β-mercaptoethanol 100U/mL penicillin, 100 mg/mL streptomycin and further supplemented with 11 mM glucose, at 37°C in a 5% CO_2 incubator. Human islets were isolated from human

cadaveric islets donors provided by the NIH/NIDDK-supported Integrated Islet Distribution Program (IIDP) (https://iidp.coh.org/overview.aspx), and from Prodo Labs (https://prodolabs.com/), the University of Miami, the University of Minnesota, the University of Wisconsin, the Southern California Islet Cell Resource enter, and the University of Edmonton, as summarized in Supplementary Table 5 Informed consent was obtained by the Organ Procurement Organization (OPO), and all donor information was de-identified in accord with Institutional Review Board procedures at The Icahn School of Medicine at Mount Sinai (ISMMS). Human islets were cultured and dispersed as previously described (14).

Adenovirus. Human islets were transduced with RIP-zsGreen at MOI of 100. Overnight, the following day, islets were dispersed, and seeded in RPMI with 100U/mL penicillin, 100 mg/mL streptomycin in the presence of additional 100 MOI AdV the virus for 2-4 hr. following, FBS was added to a final concentration of 10%, compounds added and cells were continuously imaged for the course of 48-72 hr.

Immunostaining. INS-1 cells or dispersed cells were plated on 12-mm Laminin coated glass coverslips. Cells were treated in indicated conditions and times. Cells were washed with PBS and fixed in 4% paraformaldehyde. Immunolabeling was performed as previously described (ref) with primary antibodies directed against N-terminus ChREBP [1:250, (42)], C-terminus ChREBP (Novus, 1:250), Pdx1 (Abcam, 1:500), and Insulin (Fisher, 1:1000)

qPCR and PCR. mRNA was isolated using the Qiagen RNAeasy mini kit for INS-1 cells, or for islets using the Qiagen RNAeasy mini kit. cDNA was produced using the Promega m-MLV reverse transcriptase. qPCR was performed on the QuantStudio5 using Syber-Green (BioRad) and analysis was performed using the ΔΔCt method. PCR for genotyping was performed using standard methods. Primer sequences are shown in **Table S6**.

Proximity Ligation Assay (PLA). PLA was used to determine endogenous protein–protein interactions (118-120). As previously described in (121). Briefly, ChREBPα (by GenScript) and Pan-14-3-3 (Santa Cruz) antibodies were conjugated to Duolink oligonucleotides, PLUS and MINUS oligo arms, respectively, using Duolink® In Situ Probemaker Following a PBS wash, cells were fixed with 4% formaldehyde solution for 10 min at room temperature, and blocked with Duolink Blocking Solution for 1 h at 37 °C and then incubated with 4 µg/mL ChREBPα-Plus and 14-3-3-MINUS overnight at 4 °C. PLA was performed according to the manufacturer's directions. No secondary antibodies were used, because PLUS and MINUS oligo arms were directly conjugated to ChREBP and 14-3-3. Cells were imaged on a Zeiss 510 NLO/Meta system (Zeiss, Oberkochen, Germany), using a Plan-Apochromat 63×/1.40 oil differential interference contrast objective.

Proliferation and cell death. Cellular proliferation and cell death was quantified using Real-Time Kinetic Labeling (SPARKL) technique.[22] Syto21 marked all cells, Yoyo3 marked all dead cells.

Luciferase Reporter. The reporter assays were done as described previously.[17] Briefly, INS-1-derived 832/13 cells that stably express the luciferase reporter gene under control of the human TXNIP promoter. Cells were harvested after 24 h and luciferase activity was measured using the Luciferase Reporter Assay System (Promega, Cat. #E1500) on Victor Nivo luminometer (PerkinElmer). Firefly luciferase activity was normalized to *Renilla* luciferase activity.

Statistics. All studies were performed with a minimum of three independent replications. Data were represented in this study as means ± standard error of the mean (SEM). Statistical analysis was performed using two-way ANOVA on GraphPad (Prism) V9.2.

Figure Legends:

Fig. 1: Protein-Protein Interaction between 14-3-3 and ChREBPα regulates β-cell fate. a. Under normoglycemic conditions, ChREBPα remains mostly cytoplasmic by binding to 14-3-3. ChREBPα is one of very few phosphorylation-independent 14-3-3 partner proteins and binds *via* a pocket containing a phosphate or sulfate ion, ketone, or AMP. **b.** In acute hyperglycemia, ChREBPα dissociates from 14-3-3 and transiently translocates into the nucleus where it binds multiple ChoREs and promotes adaptive β-cell expansion. **c**. In prolonged hyperglycemia or hyperglycemia combined with hyperlipidemia (glucolipotoxicity), ChREBPα initiates and maintains a feed-forward surge in ChREBPβ expression, leading to β-cell demise. **d.** Novel class of molecular glue drugs specifically stabilize ChREBPα/14-3-3 interaction, prevent surge of ChREBPβ expression in glucolipotoxicity, and protect β-cell identity and survival.

Fig. 2: SAR around analog 1 resulted in improved stabilizer 30. a. Crystal structure of compound **1** (blue sticks) in complex with 14-3-3σ (white surface) and ChREBPα (red sticks and surface). Final $2F_o$-F_c electron density contoured at 1.0σ. **b.** Interactions of **1** (blue sticks) with 14-3-3σ (white) and ChREBPα (red) residues (relevant side chains are displayed in stick representation, polar contacts are shown as black dashed lines). **c.** FA 2D protein titration of 14-3-3β in FITC-labeled ChREBPα peptide (10 nM) and varied but fixed concentrations of **1** (0–500 μM), including the cooperativity factor (α) and intrinsic affinity of **1** to 14-3-3 (K_DII). **d.** Structure and activity analogs of **1**. The two best compounds are marked in cyan and yellow. EC_{50} in parenthesis with mean ± SD, n = 2. For FA titration graphs see **Fig. S4, S5**. **e, f.** Crystallographic overlay of **1** (blue sticks) with **30** (yellow sticks) in complex of 14-3-3σ (white cartoon) and ChREBPα (red cartoon). **g.** Interactions of **30** (yellow) with 14-3-3 σ (white) and ChREBPα (red) (relevant side chains are displayed in stick representation, polar contacts are shown as black dashed lines).

Fig. 3: Fluorination of compounds enhances stabilizing potency. a. Structures and bar graphs of pEC_{50} values derived from FA compound titrations, for Y=H (blue bars) and Y=F (yellow bars). (For graphs see **Fig. S4, S5**, for EC_{50} values see **Table S2**) (mean ± SD, n=2). **b, c.** Titration of 14-3-3β to FITC-labeled ChREBPα peptide (10 nM) against varying fixed concentrations of **30** or **43** (0–500 μM) (mean ± SD, n = 2), including the cooperativity factor (α) and intrinsic affinity of the stabilizers to 14-3-3 (K_DII). **d.** Selectivity studies by titrating **43** to 14-3-3β and eight different 14-3-3 interaction FITC-labeled peptides (all 10 nM) (mean ± SD, n = 2). **e.** Crystallographic overlay **30** (yellow) and **43** (purple) in complex with 14-3-3σ (white cartoon) and ChREBPα (red cartoon). Helix 9 of 14-3-3σ is colored in the same color as the corresponding compound, showing a helical 'clamping' effect when **43** (purple) is present. **f.** Surface representation of **43** (purple) in complex with 14-3-3σ (white) and ChREBPα (red), showing the distances (black dashes) of the **43** m-F substitution to the residues (sticks) of 14-3-3σ and ChREBPα. **g.** Interactions of **43** (purple) with 14-3-3σ (white) and ChREBPα (red) (relevant side chains are displayed in stick representation, polar contacts are shown as black dashed lines).

Fig. 4: Active compounds protect human islets and human β-cell from glucolipotoxicity. a. Overview of compounds included in cellular assays. Table shows results of cytotoxicity and β-cell rescue from glucolipotoxicity in the presence of the compounds (green indicates positive outcome and red cytotoxicty). **b.** Schematic of adaptation to the SPARKL assay in human islets to specifically monitor β-cells. **c.** Representative figures from **d** at 48 h with **43**. The results are representative from 4 different human cadaveric donors. **d.** Representative kinetics of β-cell death in glucolipotoxicity (20 mM glucose+500 μM palmitate), in the presence of 10

μM of the indicated compounds. **e.** Quantification of β-cell death (assessed by Yoyo3+% of GFP+ cells) at 24 h from **d**. **f, g.** Quantification of insulin positive cells (Ins+ and Nucblue+) **f.** Kinetic representative measurement of % change in INS+ cell numbers over time. **g.** Overall change in β-cell numbers at 24 hr. Data are means +/- SEM; n=4; *, $p < 0.05$ compared to glucolipotoxicity

Fig. 5: 43 stabilizes ChREBPα/14-3-3 interaction and thus retains cytoplasmic ChREBPα localization in response to glucose and glucolipotoxicity. a. Proximity ligation assay demonstrating increased interaction between 14-3-3 and ChREBPα**.** INS-1 cells were culture for overnight (ON) at 5.5mM glucose, and exposed to high (2omM) glucose for indicated times **b, d.** Representative figures showing the nuclear localization of ChREBPα after exposure to high glucose (**b**) or glucolipotoxic (**d**) conditions. **c, e.** Time course of nuclear localization of ChREBPα based on figures **b**, **d**, respectively. **f, g.** CRISPR/Cas9 engineered INS-1 cells treated with indicated compounds for 24 hr Low-5.5 mM glucose, High-20 mM glucose; glucolipotoxicity-20 mM glucose+500 μM palmitate. **f.** Representative images at 24 hr. **g.** quantification of % nuclear ChREBP at 24 hr. Data are the means +/- SEM, n=3-5, *$p<0.05$, **$p<0.01$.

Fig. 6: 43 preserves β-cell identity in glucolipotoxicity and prevents upregulation of ChREBPβ in high glucose and glucolipotoxicity. a,b,f,g. mRNA fold enrichment over control low glucose in human islets, treated with 10 μM **43** for 24 h. Low-5.5 mM glucose, High-20 mM glucose; glucotox-20 mM glucose+500 μM palmitate. **c, d, h**. Immunostaining for PDX1, c-term ChREBP, and insulin in dispersed islets treated for 48 h with indicated treatments. **e.** INS-1 cells expressing luciferase driven by the human TXNIP promoter were incubated for 24 hr at the indicated glucose concentrations, in the presence or absence of 10 μM **43**. Data are the means +/- SEM, n=4, ***, $p<0.005$, ****, $p<0.001$. Data are the means +/- SEM, n=3-7, *$p<0.05$, **$p<0.01$.

Acknowledgments:

This work was supported by the European Union through ERC Advanced Grant PPI-Glue (101098234), the Netherlands Ministry of Education, Culture and Science (Gravity program 024.001.035). The Netherlands Organization for Scientific Research (ECHO grant 711.018.003), and by DFG-funded CRC1093 (Supramolecular Chemistry on Proteins). Views and opinions expressed are however those of the authors only and do not necessarily reflect those of the European Union or the European Research Council. Neither the European Union nor the granting authority can be held responsible for them. DKS grant support from NIH/NIDDK R01DK130300 and P30DK020541
We thank Michelle Arkin (UCSF) for stimulating discussions.

References

1. Ogurtsova K, Guariguata L, Barengo NC, Ruiz PL, Sacre JW, Karuranga S, et al. IDF diabetes Atlas: Global estimates of undiagnosed diabetes in adults for 2021. *Diabetes Res Clin Pract.* 2022;183:109118.
2. Collaborators GBDD. Global, regional, and national burden of diabetes from 1990 to 2021, with projections of prevalence to 2050: a systematic analysis for the Global Burden of Disease Study 2021. *Lancet.* 2023;402(10397):203-34.
3. The L. Diabetes: a defining disease of the 21st century. *Lancet.* 2023;401(10394):2087.
4. Dowarah J, and Singh VP. Anti-diabetic drugs recent approaches and advancements. *Bioorganic & medicinal chemistry.* 2020;28(5):115263.
5. Tancredi M, Rosengren A, Svensson A-M, Kosiborod M, Pivodic A, Gudbjörnsdottir S, et al. Excess mortality among persons with type 2 diabetes. *New England Journal of Medicine.* 2015;373(18):1720-32.
6. Chatterjee S, Khunti K, and Davies MJ. Type 2 diabetes. *The lancet.* 2017;389(10085):2239-51.
7. Schellenberg ES, Dryden DM, Vandermeer B, Ha C, and Korownyk C. Lifestyle interventions for patients with and at risk for type 2 diabetes: a systematic review and meta-analysis. *Annals of internal medicine.* 2013;159(8):543-51.
8. Martín-Peláez S, Fito M, and Castaner O. Mediterranean diet effects on type 2 diabetes prevention, disease progression, and related mechanisms. A review. *Nutrients.* 2020;12(8):2236.
9. Iizuka K, Takao K, and Yabe D. ChREBP-mediated regulation of lipid metabolism: involvement of the gut microbiota, liver, and adipose tissue. *Frontiers in endocrinology.* 2020;11:587189.
10. Ortega-Prieto P, and Postic C. Carbohydrate Sensing Through the Transcription Factor ChREBP. *Front Genet.* 2019;10:472.
11. Abdul-Wahed A, Guilmeau S, and Postic C. Sweet Sixteenth for ChREBP: Established Roles and Future Goals. *Cell Metab.* 2017;26(2):324-41.
12. Dentin R, Benhamed F, Hainault I, Fauveau V, Foufelle F, Dyck JR, et al. Liver-specific inhibition of ChREBP improves hepatic steatosis and insulin resistance in ob/ob mice. *Diabetes.* 2006;55(8):2159-70.
13. Vijayakumar A, Aryal P, Wen J, Syed I, Vazirani RP, Moraes-Vieira PM, et al. Absence of Carbohydrate Response Element Binding Protein in Adipocytes Causes Systemic Insulin Resistance and Impairs Glucose Transport. *Cell Rep.* 2017;21(4):1021-35.
14. Metukuri MR, Zhang P, Basantani MK, Chin C, Stamateris RE, Alonso LC, et al. ChREBP mediates glucose-stimulated pancreatic beta-cell proliferation. *Diabetes.* 2012;61(8):2004-15.
15. Henley MJ, and Koehler AN. Advances in targeting 'undruggable' transcription factors with small molecules. *Nat Rev Drug Discov.* 2021;20(9):669-88.
16. Song Z, Yang H, Zhou L, and Yang F. Glucose-sensing transcription factor MondoA/ChREBP as targets for type 2 diabetes: opportunities and challenges. *International Journal of Molecular Sciences.* 2019;20(20):5132.
17. Sakiyama H, Wynn RM, Lee WR, Fukasawa M, Mizuguchi H, Gardner KH, et al. Regulation of nuclear import/export of carbohydrate response element-binding protein (ChREBP): interaction of an alpha-helix of ChREBP with the 14-3-3 proteins and regulation by phosphorylation. *J Biol Chem.* 2008;283(36):24899-908.
18. Merla G, Howald C, Antonarakis SE, and Reymond A. The subcellular localization of the ChoRE-binding protein, encoded by the Williams-Beuren syndrome critical region gene 14, is regulated by 14-3-3. *Hum Mol Genet.* 2004;13(14):1505-14.
19. Somsen BA, Craenmehr FWB, Liu WW, Koops AA, Pennings MAM, Visser EJ, et al. Functional mapping of the 14-3-3 hub protein as a guide to design 14-3-3 molecular glues. *Chem Sci.* 2022;13(44):13122-31.

20. Wolter M, Valenti D, Cossar PJ, Hristeva S, Levy LM, Genski T, et al. An Exploration of Chemical Properties Required for Cooperative Stabilization of the 14-3-3 Interaction with NF-kappaB-Utilizing a Reversible Covalent Tethering Approach. *J Med Chem.* 2021;64(12):8423-36.
21. Wolter M, Valenti D, Cossar PJ, Levy LM, Hristeva S, Genski T, et al. Fragment-Based Stabilizers of Protein-Protein Interactions through Imine-Based Tethering. *Angew Chem Int Ed Engl.* 2020;59(48):21520-4.
22. Sijbesma E, Visser E, Plitzko K, Thiel P, Milroy LG, Kaiser M, et al. Structure-based evolution of a promiscuous inhibitor to a selective stabilizer of protein-protein interactions. *Nat Commun.* 2020;11(1):3954.
23. Lim GE, Piske M, and Johnson JD. 14-3-3 proteins are essential signalling hubs for beta cell survival. *Diabetologia.* 2013;56(4):825-37.
24. Mugabo Y, Zhao C, Tan JJ, Ghosh A, Campbell SA, Fadzeyeva E, et al. 14-3-3zeta Constrains insulin secretion by regulating mitochondrial function in pancreatic beta cells. *JCI Insight.* 2022;7(8).
25. Rial SA, Shishani R, Cummings BP, and Lim GE. Is 14-3-3 the Combination to Unlock New Pathways to Improve Metabolic Homeostasis and beta-Cell Function? *Diabetes.* 2023;72(8):1045-54.
26. Jiang W, Tong T, Li W, Huang Z, Chen G, Zeng F, et al. Molecular Evolution of Plant 14-3-3 Proteins and Function of Hv14-3-3A in Stomatal Regulation and Drought Tolerance. *Plant Cell Physiol.* 2023;63(12):1857-72.
27. Paul AL, Liu L, McClung S, Laughner B, Chen S, and Ferl RJ. Comparative interactomics: analysis of arabidopsis 14-3-3 complexes reveals highly conserved 14-3-3 interactions between humans and plants. *J Proteome Res.* 2009;8(4):1913-24.
28. Zhang K, Huang Y, and Shi Q. Genome-wide identification and characterization of 14-3-3 genes in fishes. *Gene.* 2021;791:145721.
29. Abdrabou A, Brandwein D, and Wang Z. Differential Subcellular Distribution and Translocation of Seven 14-3-3 Isoforms in Response to EGF and During the Cell Cycle. *Int J Mol Sci.* 2020;21(1).
30. Hermeking H, and Benzinger A. 14-3-3 proteins in cell cycle regulation. *Semin Cancer Biol.* 2006;16(3):183-92.
31. Bunney TD, van Walraven HS, and de Boer AH. 14-3-3 protein is a regulator of the mitochondrial and chloroplast ATP synthase. *Proc Natl Acad Sci U S A.* 2001;98(7):4249-54.
32. Kim D, Won J, Shin DW, Kang J, Kim YJ, Choi SY, et al. Regulation of Dyrk1A kinase activity by 14-3-3. *Biochem Biophys Res Commun.* 2004;323(2):499-504.
33. Karlberg T, Hornyak P, Pinto AF, Milanova S, Ebrahimi M, Lindberg M, et al. 14-3-3 proteins activate Pseudomonas exotoxins-S and -T by chaperoning a hydrophobic surface. *Nat Commun.* 2018;9(1):3785.
34. Ottmann C, Yasmin L, Weyand M, Veesenmeyer JL, Diaz MH, Palmer RH, et al. Phosphorylation-independent interaction between 14-3-3 and exoenzyme S: from structure to pathogenesis. *EMBO J.* 2007;26(3):902-13.
35. Toleman CA, Schumacher MA, Yu SH, Zeng W, Cox NJ, Smith TJ, et al. Structural basis of O-GlcNAc recognition by mammalian 14-3-3 proteins. *Proc Natl Acad Sci U S A.* 2018;115(23):5956-61.
36. Ge Q, Huang N, Wynn RM, Li Y, Du X, Miller B, et al. Structural characterization of a unique interface between carbohydrate response element-binding protein (ChREBP) and 14-3-3beta protein. *J Biol Chem.* 2012;287(50):41914-21.
37. Sato S, Jung H, Nakagawa T, Pawlosky R, Takeshima T, Lee WR, et al. Metabolite Regulation of Nuclear Localization of Carbohydrate-response Element-binding Protein (ChREBP): ROLE OF AMP AS AN ALLOSTERIC INHIBITOR. *J Biol Chem.* 2016;291(20):10515-27.

38. Nakagawa T, Ge Q, Pawlosky R, Wynn RM, Veech RL, and Uyeda K. Metabolite regulation of nucleo-cytosolic trafficking of carbohydrate response element-binding protein (ChREBP): role of ketone bodies. *J Biol Chem.* 2013;288(39):28358-67.
39. Pennington KL, Chan TY, Torres MP, and Andersen JL. The dynamic and stress-adaptive signaling hub of 14-3-3: emerging mechanisms of regulation and context-dependent protein-protein interactions. *Oncogene.* 2018;37(42):5587-604.
40. Herman MA, Peroni OD, Villoria J, Schon MR, Abumrad NA, Bluher M, et al. A novel ChREBP isoform in adipose tissue regulates systemic glucose metabolism. *Nature.* 2012;484(7394):333-8.
41. Katz LS, Baumel-Alterzon S, Scott DK, and Herman MA. Adaptive and maladaptive roles for ChREBP in the liver and pancreatic islets. *J Biol Chem.* 2021;296:100623.
42. Katz LS, Brill G, Zhang P, Kumar A, Baumel-Alterzon S, Honig LB, et al. Maladaptive positive feedback production of ChREBPbeta underlies glucotoxic beta-cell failure. *Nat Commun.* 2022;13(1):4423.
43. Zhang P, Kumar A, Katz LS, Li L, Paulynice M, Herman MA, and Scott DK. Induction of the ChREBPbeta Isoform Is Essential for Glucose-Stimulated beta-Cell Proliferation. *Diabetes.* 2015;64(12):4158-70.
44. Allen BK, Mehta S, Ember SW, Schonbrunn E, Ayad N, and Schurer SC. Large-Scale Computational Screening Identifies First in Class Multitarget Inhibitor of EGFR Kinase and BRD4. *Sci Rep.* 2015;5:16924.
45. Keiser MJ, Setola V, Irwin JJ, Laggner C, Abbas AI, Hufeisen SJ, et al. Predicting new molecular targets for known drugs. *Nature.* 2009;462(7270):175-81.
46. Lengauer T, Lemmen C, Rarey M, and Zimmermann M. Novel technologies for virtual screening. *Drug Discov Today.* 2004;9(1):27-34.
47. Nicolaou CA, Humblet C, Hu H, Martin EM, Dorsey FC, Castle TM, et al. Idea2Data: Toward a New Paradigm for Drug Discovery. *ACS Med Chem Lett.* 2019;10(3):278-86.
48. Shoichet BK. Virtual screening of chemical libraries. *Nature.* 2004;432(7019):862-5.
49. Zhou P, Zou J, Tian F, and Shang Z. Fluorine Bonding⊠How Does It Work In Protein− Ligand Interactions? *Journal of chemical information and modeling.* 2009;49(10):2344-55.
50. Dalvit C, Invernizzi C, and Vulpetti A. Fluorine as a hydrogen-bond acceptor: Experimental evidence and computational calculations. *Chemistry–A European Journal.* 2014;20(35):11058-68.
51. Okiyama Y, Fukuzawa K, Komeiji Y, and Tanaka S. Taking water into account with the fragment molecular orbital method. *Quantum Mechanics in Drug Discovery.* 2020:105-22.
52. Shah P, and Westwell AD. The role of fluorine in medicinal chemistry. *J Enzyme Inhib Med Chem.* 2007;22(5):527-40.
53. Purser S, Moore PR, Swallow S, and Gouverneur V. Fluorine in medicinal chemistry. *Chem Soc Rev.* 2008;37(2):320-30.
54. Geertjens NH, de Vink PJ, Wezeman T, Markvoort AJ, and Brunsveld L. A general framework for straightforward model construction of multi-component thermodynamic equilibrium systems. *bioRxiv.* 2021:2021.11. 18.469126.
55. Thiel P, Roglin L, Meissner N, Hennig S, Kohlbacher O, and Ottmann C. Virtual screening and experimental validation reveal novel small-molecule inhibitors of 14-3-3 protein-protein interactions. *Chem Commun (Camb).* 2013;49(76):8468-70.
56. Zhao J, Du Y, Horton JR, Upadhyay AK, Lou B, Bai Y, et al. Discovery and structural characterization of a small molecule 14-3-3 protein-protein interaction inhibitor. *Proc Natl Acad Sci U S A.* 2011;108(39):16212-6.
57. Wu H, Ge J, and Yao SQ. Microarray-assisted high-throughput identification of a cell-permeable small-molecule binder of 14-3-3 proteins. *Angew Chem Int Ed Engl.* 2010;49(37):6528-32.
58. Park E, Rawson S, Li K, Kim BW, Ficarro SB, Pino GG, et al. Architecture of autoinhibited and active BRAF-MEK1-14-3-3 complexes. *Nature.* 2019;575(7783):545-50.

59. Molzan M, Kasper S, Roglin L, Skwarczynska M, Sassa T, Inoue T, et al. Stabilization of physical RAF/14-3-3 interaction by cotylenin A as treatment strategy for RAS mutant cancers. *ACS Chem Biol.* 2013;8(9):1869-75.
60. Wolter M, Valenti D, Cossar PJ, Levy LM, Hristeva S, Genski T, et al. Fragment-Based Stabilizers of Protein–Protein Interactions through Imine-Based Tethering. *Angewandte Chemie International Edition.* 2020;59(48):21520-4.
61. Centorrino F, Ballone A, Wolter M, and Ottmann C. Biophysical and structural insight into the USP8/14-3-3 interaction. *FEBS Lett.* 2018;592(7):1211-20.
62. De Vries-van Leeuwen IJ, da Costa Pereira D, Flach KD, Piersma SR, Haase C, Bier D, et al. Interaction of 14-3-3 proteins with the estrogen receptor alpha F domain provides a drug target interface. *Proc Natl Acad Sci U S A.* 2013;110(22):8894-9.
63. Cossar PJ, Wolter M, van Dijck L, Valenti D, Levy LM, Ottmann C, and Brunsveld L. Reversible Covalent Imine-Tethering for Selective Stabilization of 14-3-3 Hub Protein Interactions. *J Am Chem Soc.* 2021;143(22):8454-64.
64. Andrei SA, de Vink P, Sijbesma E, Han L, Brunsveld L, Kato N, et al. Rationally Designed Semisynthetic Natural Product Analogues for Stabilization of 14-3-3 Protein-Protein Interactions. *Angew Chem Int Ed Engl.* 2018;57(41):13470-4.
65. Gelles JD, and Chipuk JE. High-Throughput Cell Death Assays with Single-Cell and Population-Level Analyses Using Real-Time Kinetic Labeling (SPARKL). *STAR Protoc.* 2020;1(1).
66. Gelles JD, Mohammed JN, Santos LC, Legarda D, Ting AT, and Chipuk JE. Single-Cell and Population-Level Analyses Using Real-Time Kinetic Labeling Couples Proliferation and Cell Death Mechanisms. *Dev Cell.* 2019;51(2):277-91 e4.
67. Wang H, Bender A, Wang P, Karakose E, Inabnet WB, Libutti SK, et al. Insights into beta cell regeneration for diabetes via integration of molecular landscapes in human insulinomas. *Nat Commun.* 2017;8(1):767.
68. Alam MS. Proximity Ligation Assay (PLA). *Curr Protoc Immunol.* 2018;123(1):e58.
69. Schulze PC, Yoshioka J, Takahashi T, He Z, King GL, and Lee RT. Hyperglycemia promotes oxidative stress through inhibition of thioredoxin function by thioredoxin-interacting protein. *Journal of Biological Chemistry.* 2004;279(29):30369-74.
70. Minn AH, Hafele C, and Shalev A. Thioredoxin-interacting protein is stimulated by glucose through a carbohydrate response element and induces beta-cell apoptosis. *Endocrinology.* 2005;146(5):2397-405.
71. Yu F-X, and Luo Y. Tandem ChoRE and CCAAT motifs and associated factors regulate Txnip expression in response to glucose or adenosine-containing molecules. *PloS one.* 2009;4(12):e8397.
72. Oslowski CM, Hara T, O'Sullivan-Murphy B, Kanekura K, Lu S, Hara M, et al. Thioredoxin-interacting protein mediates ER stress-induced β cell death through initiation of the inflammasome. *Cell metabolism.* 2012;16(2):265-73.
73. Chen J, Fontes G, Saxena G, Poitout V, and Shalev A. Lack of TXNIP protects against mitochondria-mediated apoptosis but not against fatty acid–induced ER stress–mediated β-cell death. *Diabetes.* 2010;59(2):440-7.
74. Chen J, Saxena G, Mungrue IN, Lusis AJ, and Shalev A. Thioredoxin-interacting protein: a critical link between glucose toxicity and β-cell apoptosis. *Diabetes.* 2008;57(4):938-44.
75. Son J, and Accili D. Reversing pancreatic β-cell dedifferentiation in the treatment of type 2 diabetes. *Experimental & Molecular Medicine.* 2023;55(8):1652-8.
76. Puri S, Folias AE, and Hebrok M. Plasticity and dedifferentiation within the pancreas: development, homeostasis, and disease. *Cell stem cell.* 2015;16(1):18-31.
77. Accili D, Talchai SC, Kim-Muller JY, Cinti F, Ishida E, Ordelheide AM, et al. When beta-cells fail: lessons from dedifferentiation. *Diabetes Obes Metab.* 2016;18 Suppl 1(Suppl 1):117-22.
78. Cinti F, Bouchi R, Kim-Muller JY, Ohmura Y, Sandoval PR, Masini M, et al. Evidence of beta-Cell Dedifferentiation in Human Type 2 Diabetes. *J Clin Endocrinol Metab.* 2016;101(3):1044-54.

79. Wysham C, and Shubrook J. Beta-cell failure in type 2 diabetes: mechanisms, markers, and clinical implications. *Postgrad Med.* 2020;132(8):676-86.
80. Song Z, Yang H, Zhou L, and Yang F. Glucose-Sensing Transcription Factor MondoA/ChREBP as Targets for Type 2 Diabetes: Opportunities and Challenges. *Int J Mol Sci.* 2019;20(20).
81. Lu J, Qian Y, Altieri M, Dong H, Wang J, Raina K, et al. Hijacking the E3 ubiquitin ligase cereblon to efficiently target BRD4. *Chemistry & biology.* 2015;22(6):755-63.
82. Hines J, Lartigue S, Dong H, Qian Y, and Crews CM. MDM2-recruiting PROTAC offers superior, synergistic antiproliferative activity via simultaneous degradation of BRD4 and stabilization of p53. *Cancer research.* 2019;79(1):251-62.
83. Samarasinghe KT, An E, Genuth MA, Chu L, Holley SA, and Crews CM. OligoTRAFTACs: a generalizable method for transcription factor degradation. *RSC Chemical Biology.* 2022;3(9):1144-53.
84. Xu G, Chen J, Jing G, and Shalev A. Preventing beta-cell loss and diabetes with calcium channel blockers. *Diabetes.* 2012;61(4):848-56.
85. Cha-Molstad H, Saxena G, Chen J, and Shalev A. Glucose-stimulated expression of Txnip is mediated by carbohydrate response element-binding protein, p300, and histone H4 acetylation in pancreatic beta cells. *J Biol Chem.* 2009;284(25):16898-905.
86. Chen J, Saxena G, Mungrue IN, Lusis AJ, and Shalev A. Thioredoxin-interacting protein: a critical link between glucose toxicity and beta-cell apoptosis. *Diabetes.* 2008;57(4):938-44.
87. Borowiec AM, Własczczuk A, Olakowska E, and Lewin-Kowalik J. TXNIP inhibition in the treatment of diabetes. Verapamil as a novel therapeutic modality in diabetic patients. *Medicine and Pharmacy Reports.* 2022;95(3):243.
88. Couper J. Preserving Pancreatic Beta Cell Function in Recent-Onset Type 1 Diabetes. *JAMA.* 2023;329(12):978-9.
89. Forlenza GP, McVean J, Beck RW, Bauza C, Bailey R, Buckingham B, et al. Effect of Verapamil on Pancreatic Beta Cell Function in Newly Diagnosed Pediatric Type 1 Diabetes: A Randomized Clinical Trial. *JAMA.* 2023;329(12):990-9.
90. Meier JJ, Butler AE, Saisho Y, Monchamp T, Galasso R, Bhushan A, et al. Beta-cell replication is the primary mechanism subserving the postnatal expansion of beta-cell mass in humans. *Diabetes.* 2008;57(6):1584-94.
91. Wang P, Fiaschi-Taesch NM, Vasavada RC, Scott DK, Garcia-Ocana A, and Stewart AF. Diabetes mellitus--advances and challenges in human beta-cell proliferation. *Nat Rev Endocrinol.* 2015;11(4):201-12.
92. Kawaguchi T, Takenoshita M, Kabashima T, and Uyeda K. Glucose and cAMP regulate the L-type pyruvate kinase gene by phosphorylation/dephosphorylation of the carbohydrate response element binding protein. *Proc Natl Acad Sci U S A.* 2001;98(24):13710-5.
93. Kawaguchi T, Osatomi K, Yamashita H, Kabashima T, and Uyeda K. Mechanism for fatty acid "sparing" effect on glucose-induced transcription: regulation of carbohydrate-responsive element-binding protein by AMP-activated protein kinase. *J Biol Chem.* 2002;277(6):3829-35.
94. Ge Q, Nakagawa T, Wynn RM, Chook YM, Miller BC, and Uyeda K. Importin-alpha protein binding to a nuclear localization signal of carbohydrate response element-binding protein (ChREBP). *J Biol Chem.* 2011;286(32):28119-27.
95. Jung H, Takeshima T, Nakagawa T, MacMillan KS, Wynn RM, Wang H, et al. The structure of importin alpha and the nuclear localization peptide of ChREBP, and small compound inhibitors of ChREBP-importin alpha interactions. *Biochem J.* 2020;477(17):3253-69.
96. Huang C, Zhang Y, Kelly DJ, Tan CY, Gill A, Cheng D, et al. Thioredoxin interacting protein (TXNIP) regulates tubular autophagy and mitophagy in diabetic nephropathy through the mTOR signaling pathway. *Sci Rep.* 2016;6:29196.
97. Yoshioka J, Schulze PC, Cupesi M, Sylvan JD, MacGillivray C, Gannon J, et al. Thioredoxin-interacting protein controls cardiac hypertrophy through regulation of thioredoxin activity. *Circulation.* 2004;109(21):2581-6.

98. Domingues A, Jolibois J, Marquet de Rouge P, and Nivet-Antoine V. The Emerging Role of TXNIP in Ischemic and Cardiovascular Diseases; A Novel Marker and Therapeutic Target. *Int J Mol Sci.* 2021;22(4).
99. Guo S, Zheng F, Qiu X, and Yang N. ChREBP gene polymorphisms are associated with coronary artery disease in Han population of Hubei province. *Clin Chim Acta.* 2011;412(19-20):1854-60.
100. Denechaud PD, Dentin R, Girard J, and Postic C. Role of ChREBP in hepatic steatosis and insulin resistance. *FEBS Lett.* 2008;582(1):68-73.
101. Calle RA, Amin NB, Carvajal-Gonzalez S, Ross TT, Bergman A, Aggarwal S, et al. ACC inhibitor alone or co-administered with a DGAT2 inhibitor in patients with non-alcoholic fatty liver disease: two parallel, placebo-controlled, randomized phase 2a trials. *Nat Med.* 2021;27(10):1836-48.
102. Huchet QA, Kuhn B, Wagner B, Kratochwil NA, Fischer H, Kansy M, et al. Fluorination Patterning: A Study of Structural Motifs That Impact Physicochemical Properties of Relevance to Drug Discovery. *J Med Chem.* 2015;58(22):9041-60.
103. Prakash GS, and Wang F. Fluorine: the new kingpin of drug discovery. *chim oggi/Chem Today.* 2012;30:30-6.
104. Richardson P. Fluorination methods for drug discovery and development. *Expert Opin Drug Discov.* 2016;11(10):983-99.
105. Yerien DE, Bonesi S, and Postigo A. Fluorination methods in drug discovery. *Org Biomol Chem.* 2016;14(36):8398-427.
106. Crespo A, Rodriguez-Granillo A, and Lim VT. Quantum-Mechanics Methodologies in Drug Discovery: Applications of Docking and Scoring in Lead Optimization. *Curr Top Med Chem.* 2017;17(23):2663-80.
107. Inoue M, Sumii Y, and Shibata N. Contribution of Organofluorine Compounds to Pharmaceuticals. *ACS Omega.* 2020;5(19):10633-40.
108. Nair AS, Singh AK, Kumar A, Kumar S, Sukumaran S, Koyiparambath VP, et al. FDA-approved trifluoromethyl group-containing Drugs: A review of 20 years. *Processes.* 2022;10(10):2054.
109. Kabsch W. xds. *Acta Crystallographica Section D: Biological Crystallography.* 2010;66(2):125-32.
110. Winter G, Waterman DG, Parkhurst JM, Brewster AS, Gildea RJ, Gerstel M, et al. DIALS: implementation and evaluation of a new integration package. *Acta Crystallogr D Struct Biol.* 2018;74(Pt 2):85-97.
111. Potterton L, Agirre J, Ballard C, Cowtan K, Dodson E, Evans PR, et al. CCP4i2: the new graphical user interface to the CCP4 program suite. *Acta Crystallogr D Struct Biol.* 2018;74(Pt 2):68-84.
112. Evans PR, and Murshudov GN. How good are my data and what is the resolution? *Acta Crystallogr D Biol Crystallogr.* 2013;69(Pt 7):1204-14.
113. Vagin A, and Teplyakov A. Molecular replacement with MOLREP. *Acta Crystallogr D Biol Crystallogr.* 2010;66(Pt 1):22-5.
114. Emsley P, and Cowtan K. Coot: model-building tools for molecular graphics. *Acta Crystallogr D Biol Crystallogr.* 2004;60(Pt 12 Pt 1):2126-32.
115. Long F, Nicholls RA, Emsley P, Graaeulis S, Merkys A, Vaitkus A, and Murshudov GN. AceDRG: a stereochemical description generator for ligands. *Acta Crystallogr D Struct Biol.* 2017;73(Pt 2):112-22.
116. Murshudov GN, Skubak P, Lebedev AA, Pannu NS, Steiner RA, Nicholls RA, et al. REFMAC5 for the refinement of macromolecular crystal structures. *Acta Crystallogr D Biol Crystallogr.* 2011;67(Pt 4):355-67.
117. Joosten RP, Joosten K, Murshudov GN, and Perrakis A. PDB_REDO: constructive validation, more than just looking for errors. *Acta Crystallogr D Biol Crystallogr.* 2012;68(Pt 4):484-96.
118. Bagchi S, Fredriksson R, and Wallen-Mackenzie A. In Situ Proximity Ligation Assay (PLA). *Methods Mol Biol.* 2015;1318:149-59.

119. Gajadhar A, and Guha A. A proximity ligation assay using transiently transfected, epitope-tagged proteins: application for in situ detection of dimerized receptor tyrosine kinases. *Biotechniques.* 2010;48(2):145-52.
120. Zhu X, Zelmer A, and Wellmann S. Visualization of Protein-protein Interaction in Nuclear and Cytoplasmic Fractions by Co-immunoprecipitation and In Situ Proximity Ligation Assay. *J Vis Exp.* 2017(119).
121. Katz LS, Argmann C, Lambertini L, and Scott DK. T3 and glucose increase expression of phosphoenolpyruvate carboxykinase (PCK1) leading to increased beta-cell proliferation. *Mol Metab.* 2022;66:101646.

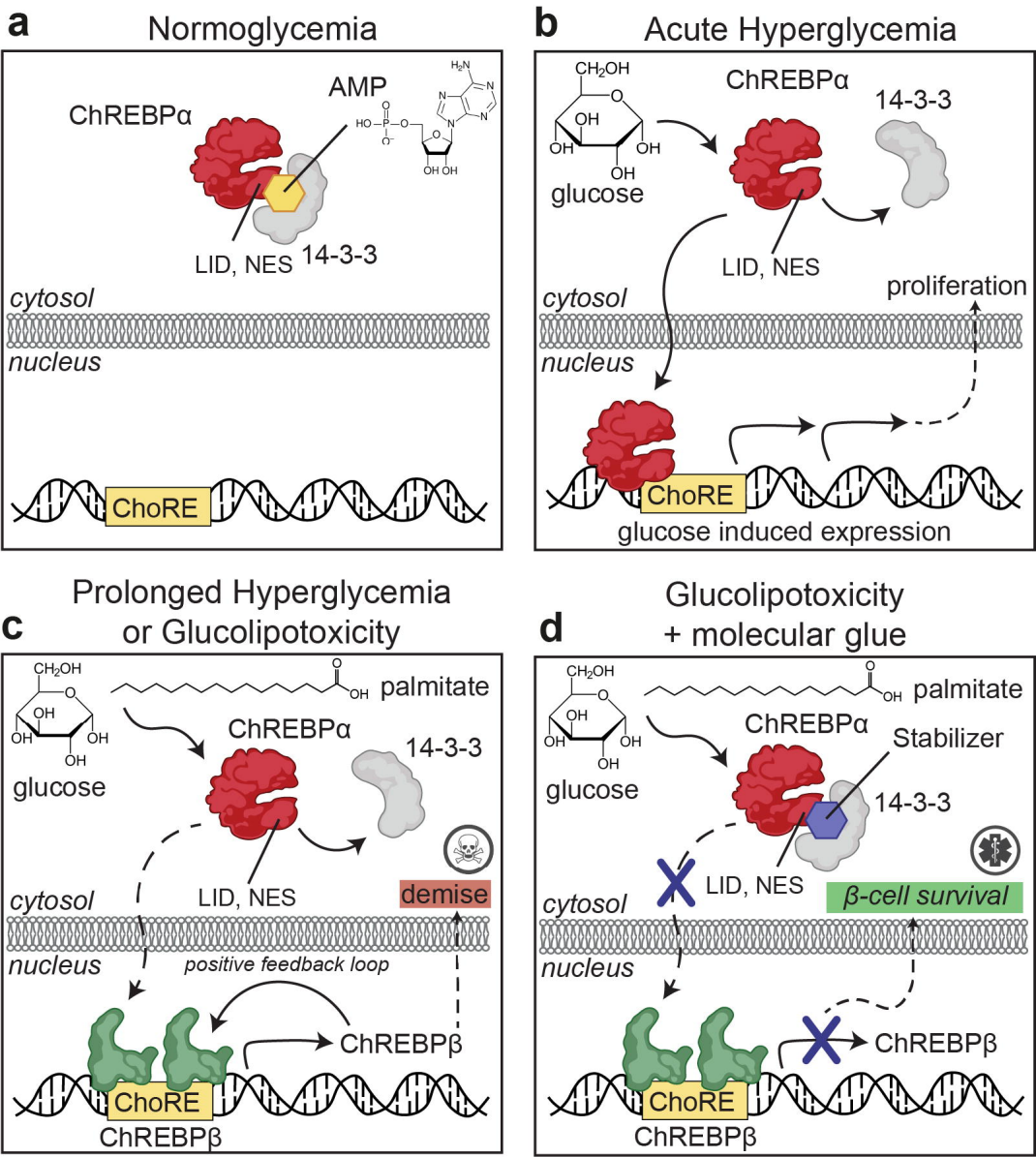
a
Normoglycemia
ChREBPα
AMP
LID, NES
14-3-3
cytosol
nucleus
ChoRE
b
Acute Hyperglycemia
glucose
ChREBPα
14-3-3
LID, NES
proliferation
cytosol
nucleus
ChoRE
glucose induced expression
c
Prolonged Hyperglycemia
or Glucolipotoxicity
palmitate
glucose
ChREBPα
14-3-3
LID, NES
demise
cytosol
nucleus
positive feedback loop
ChREBPβ
ChoRE
ChREBPβ
d
Glucolipotoxicity
+ molecular glue
palmitate
glucose
ChREBPα
Stabilizer
14-3-3
LID, NES
β-cell survival
cytosol
nucleus
ChREBPβ
ChoRE
ChREBPβ

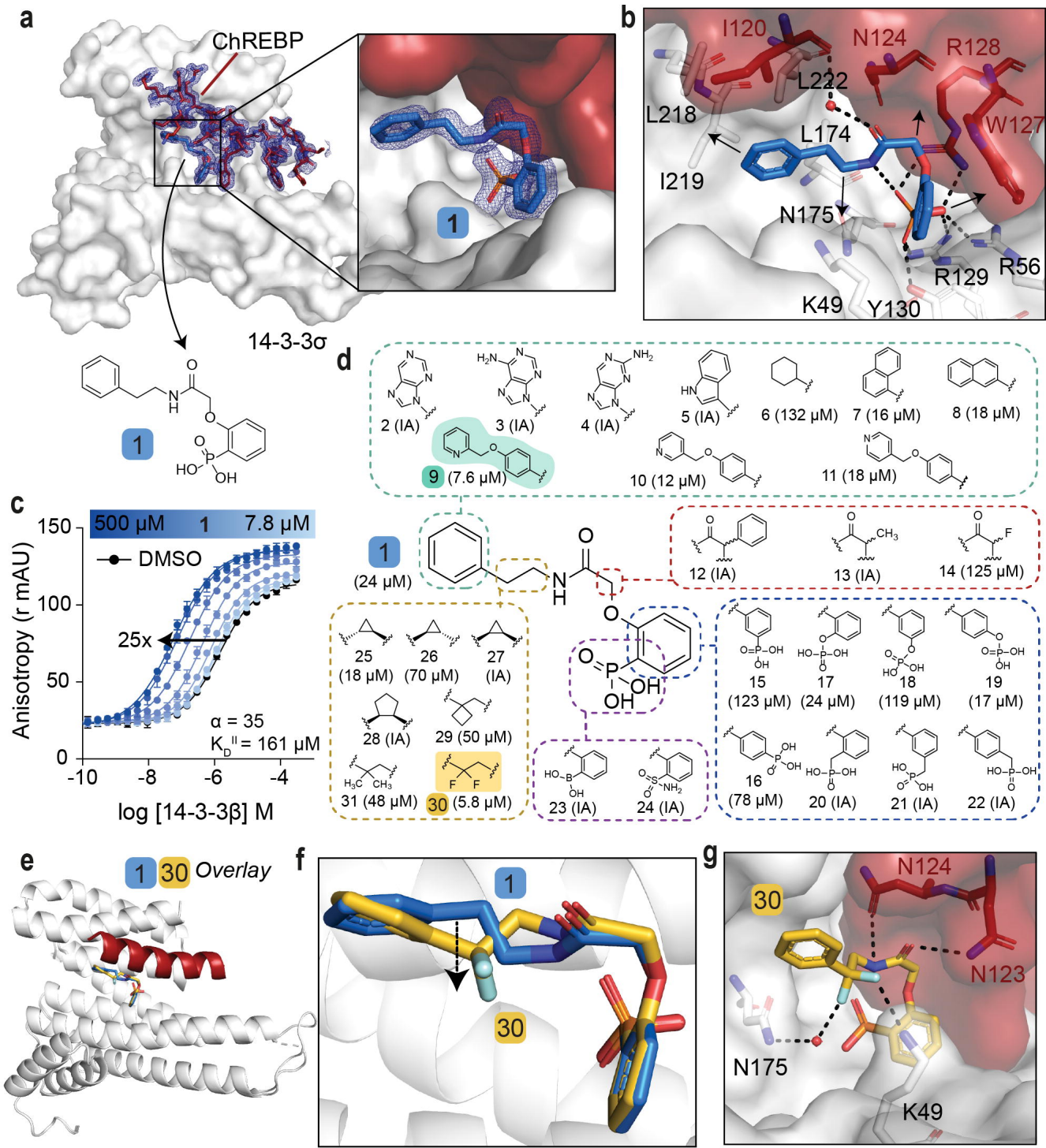
a
ChREBP
1
14-3-3σ
b
I120
N124
R128
L222
L218
L174
W127
I219
N175
R129
R56
K49
Y130
c
500 μM
1
7.8 μM
DMSO
25x
α = 35
K_D^{II} = 161 μM
Anisotropy (r mAU)
log [14-3-3β] M
d
2 (IA)
3 (IA)
4 (IA)
5 (IA)
6 (132 μM)
7 (16 μM)
8 (18 μM)
9 (7.6 μM)
10 (12 μM)
11 (18 μM)
1 (24 μM)
12 (IA)
13 (IA)
14 (125 μM)
25 (18 μM)
26 (70 μM)
27 (IA)
28 (IA)
29 (50 μM)
31 (48 μM)
30 (5.8 μM)
23 (IA)
24 (IA)
15 (123 μM)
17 (24 μM)
18 (119 μM)
19 (17 μM)
16 (78 μM)
20 (IA)
21 (IA)
22 (IA)
e
1 30 Overlay
f
1
30
g
30
N124
N123
N175
K49

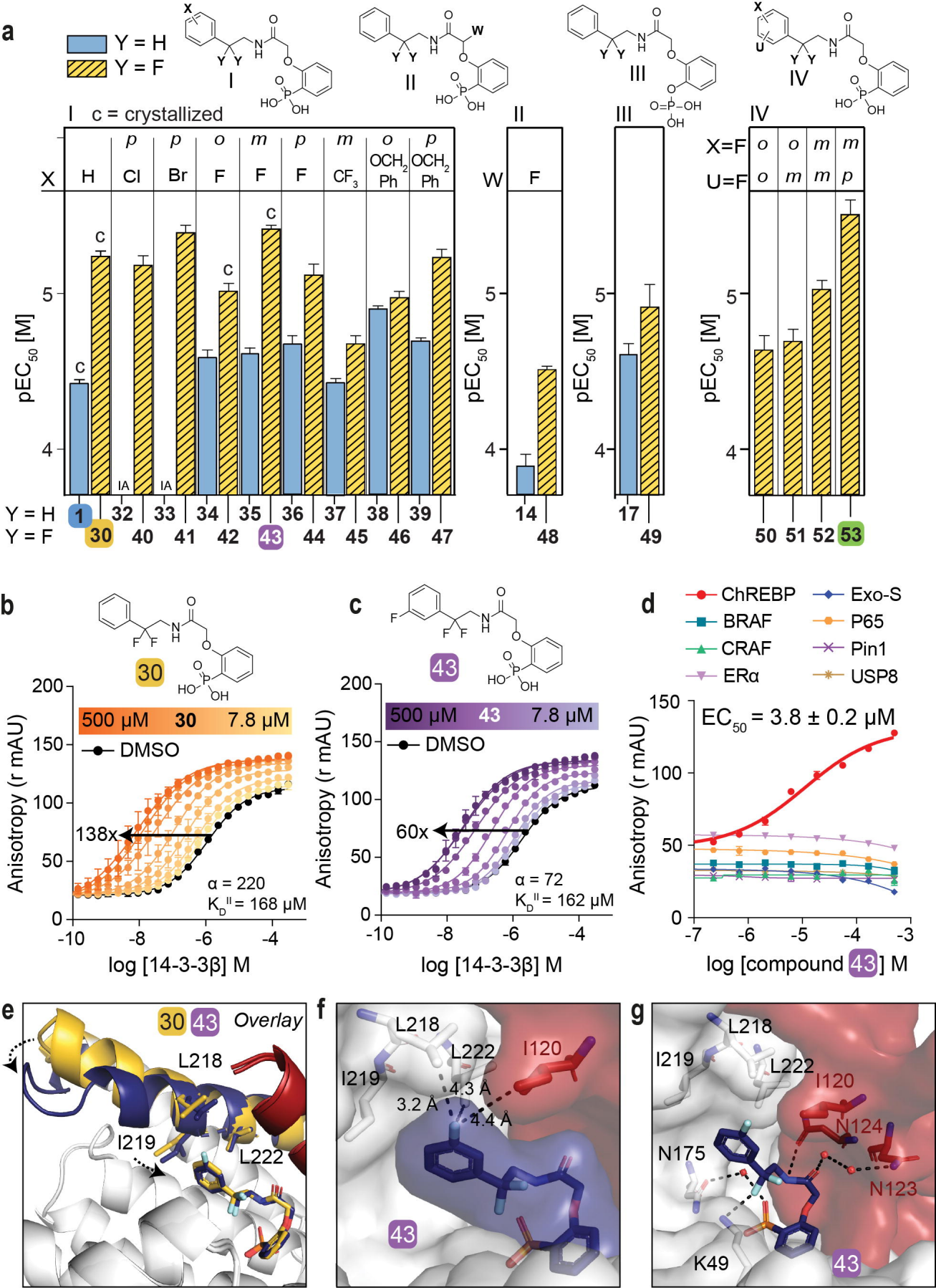
a
Y = H
Y = F
I
II
III
IV
c = crystallized
X
H
Cl
Br
F
F
F
CF3
OCH2 Ph
OCH2 Ph
W
F
X=F
U=F
pEC50 [M]
Y = H
Y = F
b
30
500 μM 30 7.8 μM
DMSO
138x
α = 220
KD" = 168 μM
Anisotropy (r mAU)
log [14-3-3β] M
c
43
500 μM 43 7.8 μM
DMSO
60x
α = 72
KD" = 162 μM
d
ChREBP
BRAF
CRAF
ERα
Exo-S
P65
Pin1
USP8
EC50 = 3.8 ± 0.2 μM
log [compound 43] M
e
30 43 Overlay
L218
I219
L222
f
L218
L222
I120
I219
4.3 Å
3.2 Å
4.4 Å
43
g
L218
I219
L222
I120
N124
N175
N123
K49
43

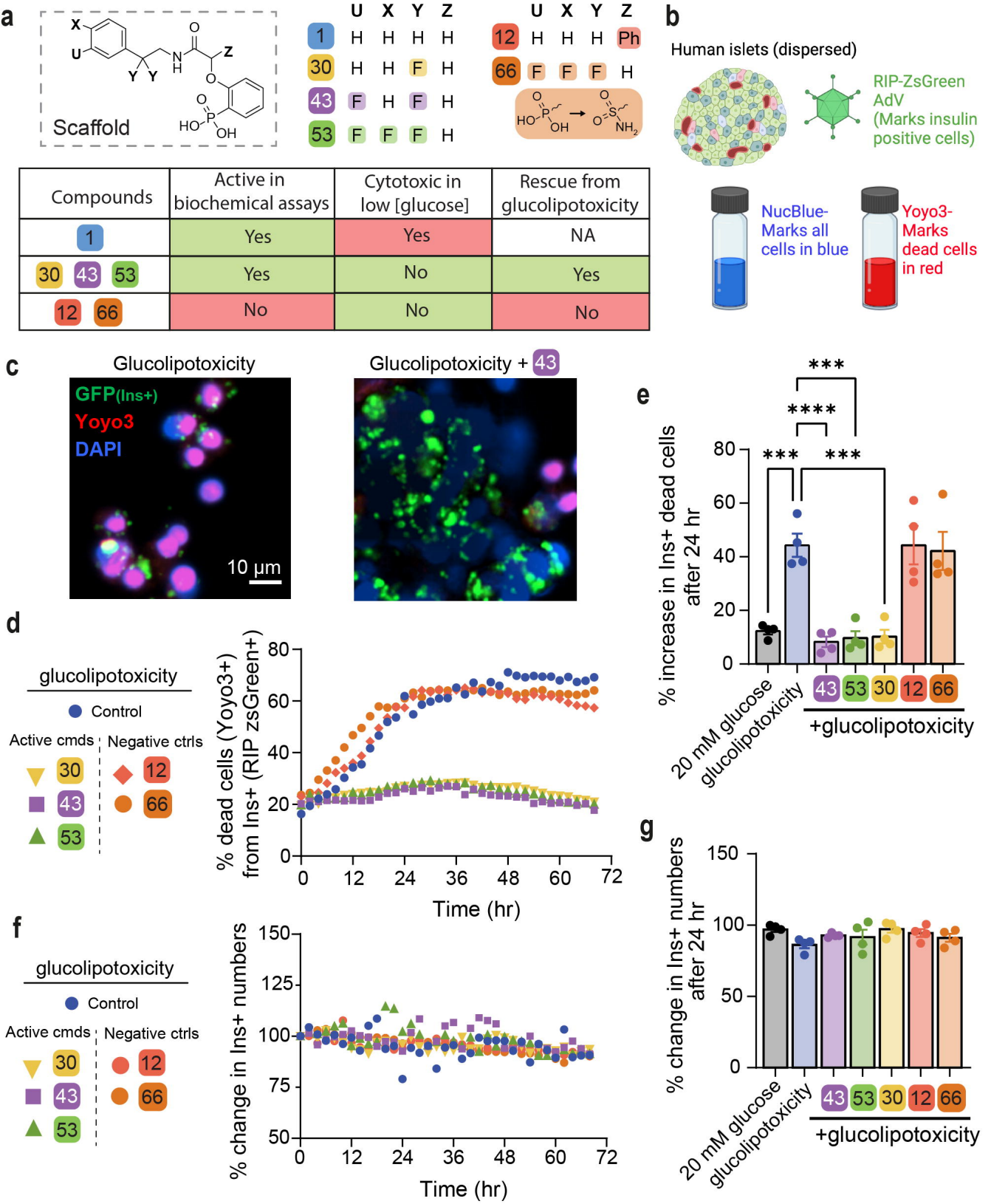

Compounds	Active in biochemical assays	Cytotoxic in low [glucose]	Rescue from glucolipotoxicity
1	Yes	Yes	NA
30 43 53	Yes	No	Yes
12 66	No	No	No

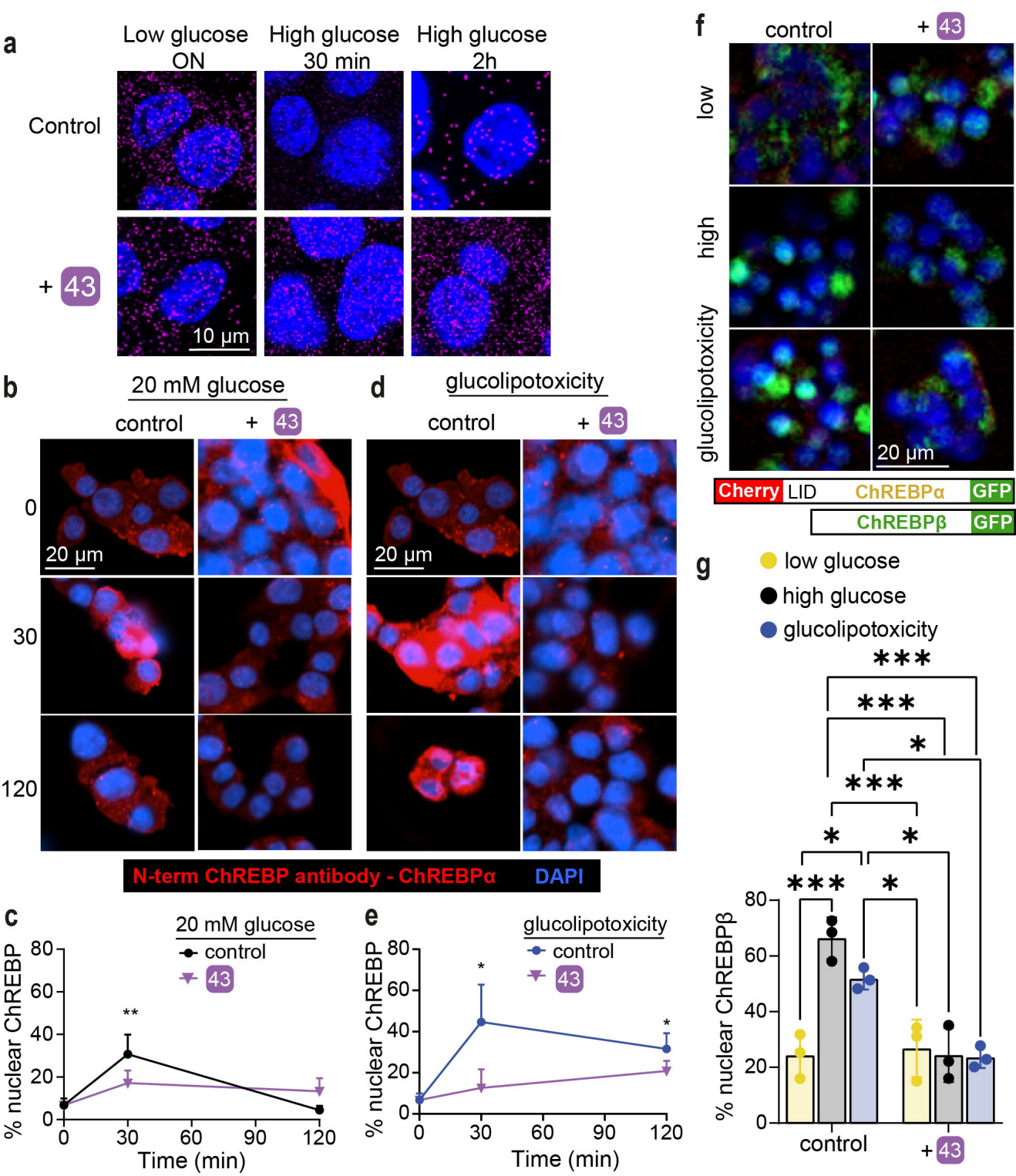
a
Low glucose ON
High glucose 30 min
High glucose 2h
Control
+ 43
10 µm
b
20 mM glucose
control
+ 43
0
30
120
20 µm
d
glucolipotoxicity
control
+ 43
20 µm
N-term ChREBP antibody - ChREBPα
DAPI
c
20 mM glucose
control
43
% nuclear ChREBP
Time (min)
e
glucolipotoxicity
control
43
% nuclear ChREBP
Time (min)
f
control
+ 43
low
high
glucolipotoxicity
20 µm
Cherry
LID
ChREBPα
GFP
ChREBPβ
GFP
g
low glucose
high glucose
glucolipotoxicity
% nuclear ChREBPβ
control
+ 43

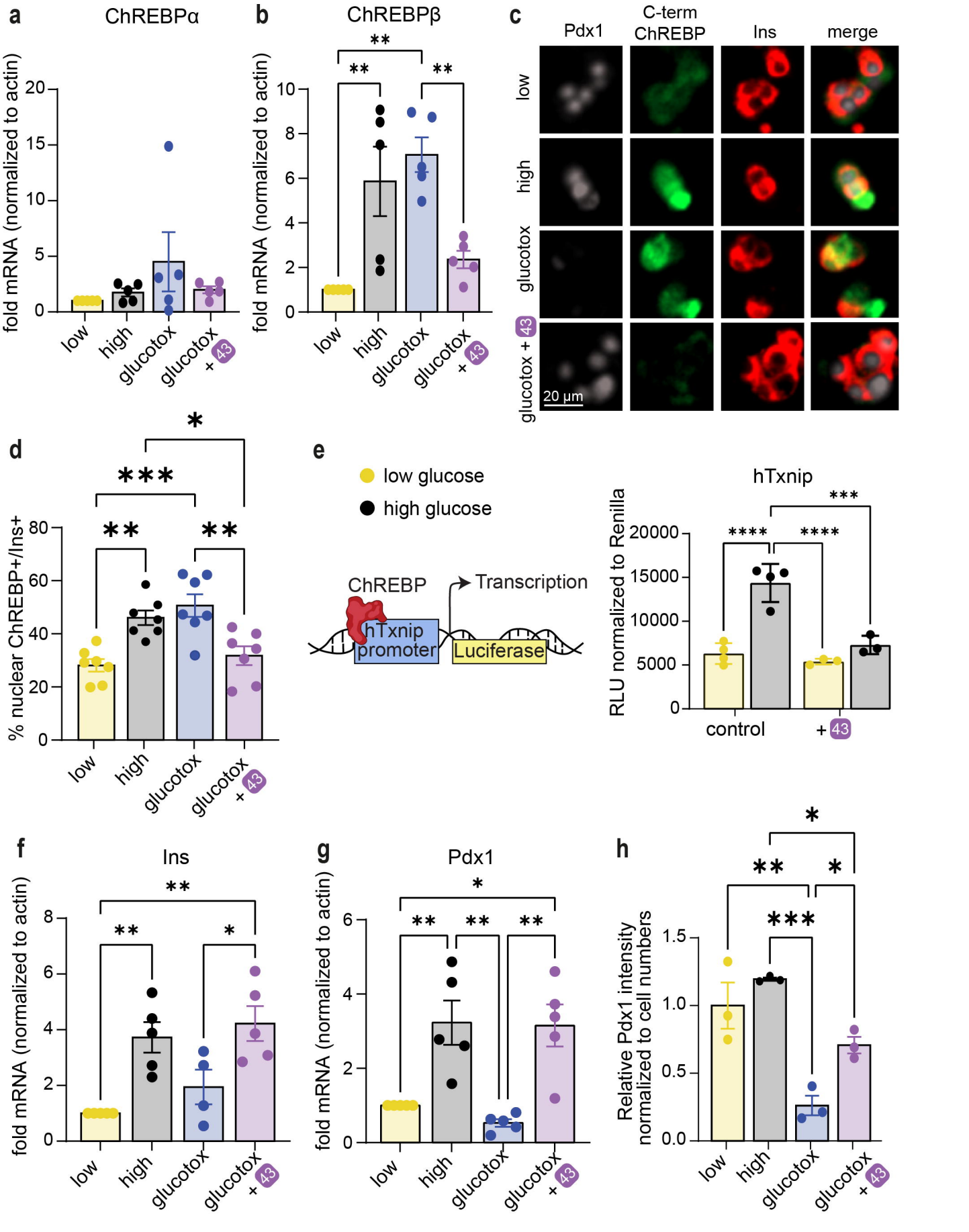
a
ChREBPα
fold mRNA (normalized to actin)
low
high
glucotox
glucotox + 43
b
ChREBPβ
fold mRNA (normalized to actin)
c
Pdx1
C-term ChREBP
Ins
merge
low
high
glucotox
glucotox + 43
20 µm
d
% nuclear ChREBP+/Ins+
e
low glucose
high glucose
ChREBP
Transcription
hTxnip promoter
Luciferase
hTxnip
RLU normalized to Renilla
control
+ 43
f
Ins
fold mRNA (normalized to actin)
g
Pdx1
fold mRNA (normalized to actin)
h
Relative Pdx1 intensity normalized to cell numbers